A new series of bioactive Mo(V)2O2S2-based thiosemicarbazone complexes: Solution and DFT studies, and antifungal and antioxidant activities

Diana Cebotari, Jordi Buils, Olga S. Garbuz, Greta G. Balan, Jérôme C. Marrot, Vincent Guérineau, David Touboul, Mohamed Haouas, Mireia Segado-Centelles, Carles Bo, et al.

A new series of bioactive $Mo^{V}_2O_2S_2$-based thiosemicarbazone complexes: Solution and DFT studies, and antifungal and antioxidant activities

Diana Cebotari,[a,b] Jordi Buils,[c] Olga Garbuz,[d] Greta Balan,[b] Jérôme Marrot,[a] Vincent Guérineau,[e] David Touboul,[e] Mohamed Haouas,[a] Mireia Segado Centellas,[c] Carles Bo,*[,c] Aurelian Gulea,*[,b] Sébastien Floquet,*[,a]

a. *Institute Lavoisier de Versailles, CNRS UMR 8180, Univ. Versailles Saint Quentin en Yvelines, Université Paris-Saclay, 45 av. des Etats-Unis, 78035 Versailles cedex (France)*
b. *State University of Moldova, 60 Alexei Mateevici str., MD-2009 Chisinau, Republic of Moldova.*
c. *Institute of Chemical Research of Catalonia (ICIQ). The Barcelona Institute of Science and Technology. Av. Països Catalans 16, 43007 Tarragona, Spain.*
d. *Institute of Zoology, 1 Academiei str., MD-2028 Chisinau, Republic of Moldova.*
e. *Université Paris-Saclay, CNRS, Institut de Chimie des Substances Naturelles, UPR 2301, 91198, Gif-sur-Yvette, France*

Corresponding author's E-mails: sebastien.floquet@uvsq.fr, guleaaurelian@gmail.com, cbo@iciq.cat

Abstract

This paper deals with the synthesis, characterization, and studies of biological properties of a series of 5 coordination compounds based on binuclear core $[Mo^{V}_2O_2S_2]^{2+}$ with thiosemicarbazones ligands bearing different substituents on the R^1 position of the ligand. The complexes are first studied using MALDI-TOF mass spectrometry and NMR spectroscopy to determine their structures in solution in relation to single-crystal X-Ray diffraction data. In a second part, the antifungal and antioxidative activities are explored and the high potential of these coordination compounds compared to the uncoordinated ligands is demonstrated for these properties. Finally, DFT calculation provides important support to the solution studies by identifying the most stable isomers in each $[Mo_2O_2S_2]^{2+}$/Ligand system, while the determination of HUMO and LUMO levels is performed to explain the antioxidative properties of these systems.

Keywords: Molybdenum, cluster, thiosemicarbazone, coordination complex, antioxidant, antifungal

Graphical abstract

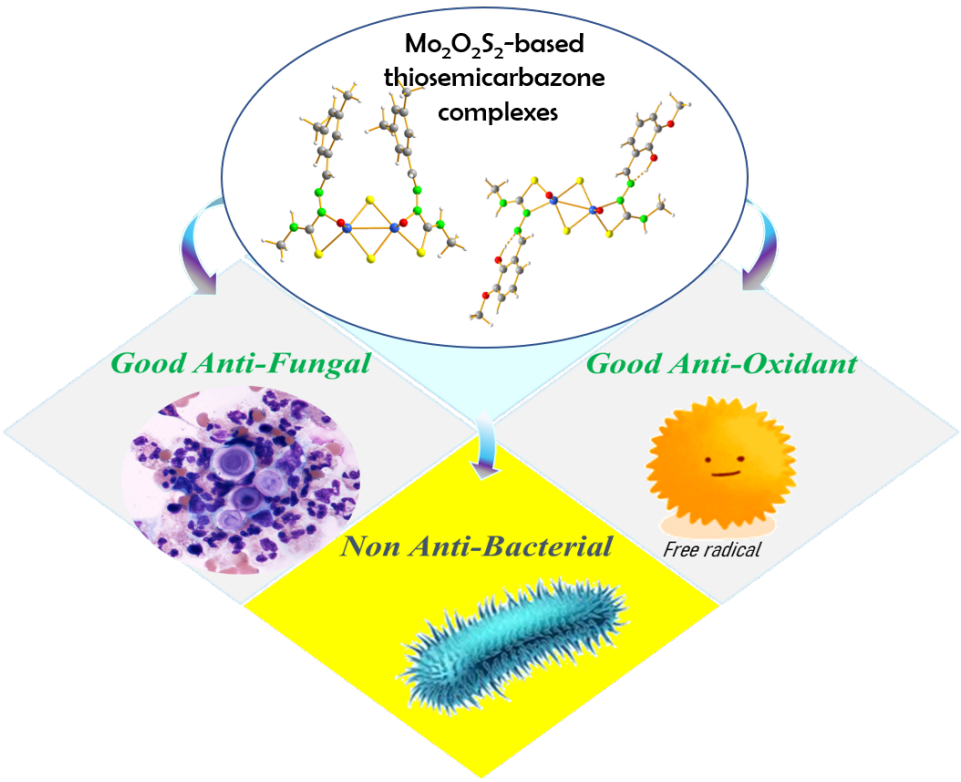

Synopsis:

Screening tests of molybdenum complexes reveal high antioxidant capacities and selective activity against fungi of the species *Cryptococcus neoformans*.

Highlights:

- $[Mo_2O_2S_2]^{2+}$-based thiosemicarbazone complexes exhibit selective fungicidal activity against the fungus *Cryptococcus neoformans*
- The strong antioxidative properties of thiosemicarbazone ligands and $[Mo_2O_2S_2]^{2+}$-based thiosemicarbazone complexes are superior to TROLOX.
- DFT calculation brings strong support for understanding the behaviour of our complexes in solution and to evidence the antioxidative properties of their ligands.

1. Introduction

Molybdenum (Mo) is present as trace element everywhere in nature, both in soils and in living organisms. Present in more than 50 enzymes, this element plays a crucial role in many biological processes, such as nitrogen assimilation by plants.[1]–[3] The molybdoenzymes typically involve Mo atoms as Mo(+VI) cations and the coordination sphere around Mo generally includes O, N and S atoms, but Mo(+VI) can be reduced into Mo(+V) and/or Mo(+IV) during biological processes. This chemical richness and its implication in biology have prompted many authors to develop biomimetic Mo-based coordination complexes. In particular, many coordination complexes based on clusters $[Mo^{V}_2O_2E_2]^{2+}$ (E = S or O) have been developed as biomimetic models for enzymes since the 1960s.[4]–[6] Surprisingly, the biological properties of such complexes have only recently been studied, including by the group of Suman and some of us. [7]–[11]

On the other hand, thiosemicarbazone ligands constitute a fascinating class of polydentate organic ligands of general formula $R^1R^2C{=}N\text{-}NH\text{-}CS\text{-}NR^3R^4$ (see scheme 1) for which chemists can easily play on the nature of substituents R^1, R^2, R^3 and R^4. This offers a huge panel of ligands capable of giving thousands of coordination complexes with transition metals.[12]–[15]

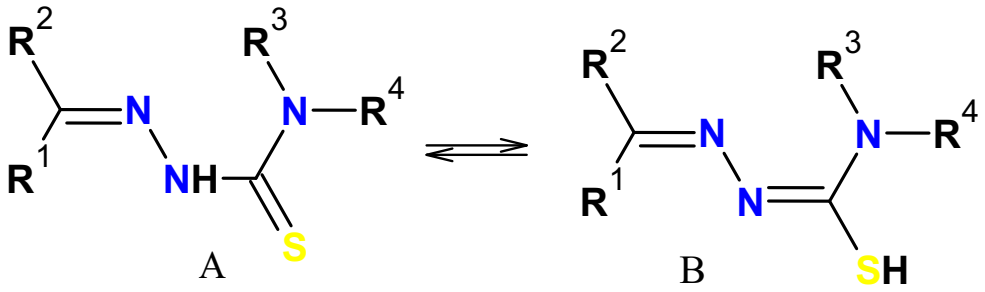

Scheme 1. *General representation of thiosemicarbazone ligand in its two forms (Thione A and Thiol B). The free ligands are usually in the A form, while the coordinated ligands are usually found in the deprotonated state of the B form.*

These coordination complexes have received considerable attention in many fields, such as biology and medicine, and the high potential of these ligands and complexes with transition metals as antitumor, antiviral, antimalarial, antibacterial, antifungal or antioxidant agents has been demonstrated.[16]–[25] Interestingly, despite the very large number of transition metal thiosemicarbazone complexes reported in the literature, molybdenum complexes are much rarer and often reported with Mo^{VI}-dioxo moieties such as $MoO_2(L)$–type complexes (where L is a tridentate thiosemicarbazone ligand), exhibiting antioxidant,[26] antitumoral[27] and antibacterial[28] properties. Mo(+V) complexes are very scarce,[29]–[32] which recently prompted us to develop a new family of $[Mo^{V}_2O_2S_2]^{2+}$-based thiosemicarbazones complexes with a wide panel of thiosemicarbazone ligands bearing various R^1, R^2, R^3 and R^4 substituents.[33] Interestingly, 14 new complexes combining $[Mo^{V}_2O_2S_2]^{2+}$ and these ligands have thus been obtained and characterized in the solid state and in solution revealing unusual coordination modes of thiosemicarbazone ligands. As a general feature, the monoprotonated ligands acted as bidentate N,S ligands with the cluster $[Mo^{V}_2O_2S_2]^{2+}$ to give essentially neutral complexes of stoichiometry cluster:ligand = 1:2. Some examples of structures obtained in our previous work are depicted in Figure 1. Studies of this new class of $[Mo^{V}_2O_2S_2]^{2+}$-thiosemicarbazone complexes showed that the R^1 group never participates in the coordination with Mo, even when it contains an aldehyde or a ketone with a phenol or a pyridine group, which contrasts with classical 3d transition metal complexes. Furthermore, we have shown that the nature of R^2 also plays an important role. Indeed, when R^2 = H, the formation of two isomers in solution in *cis* and *trans* configurations is systematically observed (see Figure 1), while the imino group remains uncoordinated, which is also unusual. Conversely, when R^2 = Me, we identified up to 8 isomers in the mixture, probably with different coordination modes. Finally, we chose to keep R^3 = H and to vary R^4 with various substituents. This position does not play a crucial role in the

formation of complexes excepted for one ligand when R^4 is an aromatic amide (Figure 1d) which gave an original tetrameric complex together with other complexes in solution.

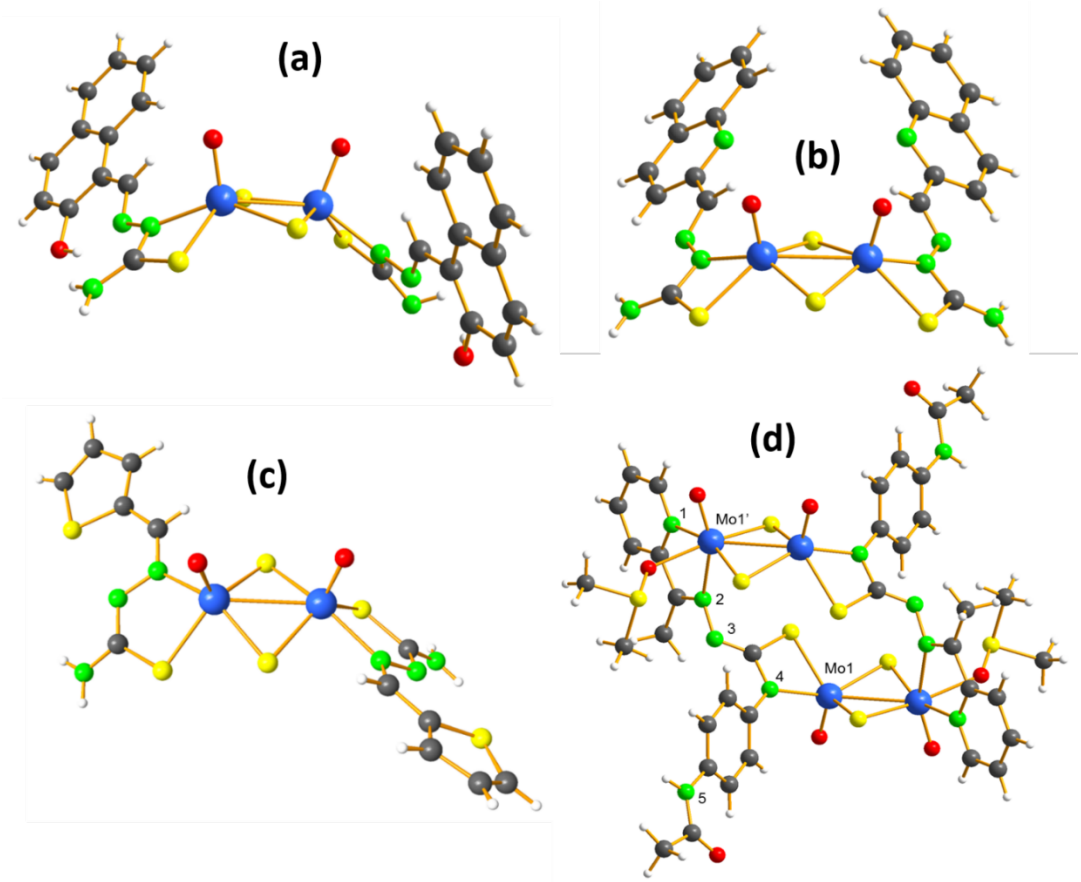

Figure 1. *Molecular structures of previous complexes a) $[Mo_2O_2S_2(HL^l)_2]$ (cis isomer), b) $[Mo_2O_2S_2(L^g)_2]$ (trans isomer), c) $[Mo_2O_2S_2(L^m)_2]$ (trans isomer) and d) $[Mo_2O_2S_2(L^f)(DMSO)]_2$ (dimer), where HL^l is defined for R^1 = H, R^2 = $C_{10}H_7O$, R^3 = H, R^4 = H, L^g with R^1 = H, R^2 = C_9H_6N, R^3 = H, R^4 = H, L^m with R^1 = H, R^2 = C_4H_3S, R^3 = H, R^4 = H, and L^f with R^1 = CH_3, R^2 = C_5H_4N, R^3 = H, R^4 = C_8H_8NO, from Fuior et al.*[33]

Very recently, the potential in biology for these 14 new complexes were screened by Fuior et al. as antibacterial, antimicrobial, antifungal, antioxidant and antitumoral compounds.[34] It was evidenced that the $Mo_2O_2S_2$-based thiosemicarbazone complexes are of interest for biology and that the activity strongly depends on the nature of the R^1 group. When R^1 is a pyridine ring, a good activity as antifungal and antimicrobial is measured, while when R^1 is a phenol the antitumoral properties are enhanced. It is worth noting that for antifungal activity a good activity against *Cryptococcus neoformans* is measured for all complexes, while the activity

against *Candida albicans* appears good only for complexes bearing pyridine derivatives. Besides, the formation of mixtures of isomers constitutes a severe drawback for the interpretation of results in biology and ligands alone were only partially measured, which does not permit to establish if the main contribution of the properties come from the ligand or from the molybdenum cluster. Finally, all complexes exhibit antioxidant properties better than TROLOX, the reference compound commonly used in the literature, but the properties of ligands alone were not measured, and the origin of the process was not established.

The present study aims to address the issues evidenced by Fuior et al with this new class of $Mo_2O_2S_2$-based thiosemicarbazone complexes[33][34]:

- Controlling the formation of mixtures of isomers by introducing steric constraints.
- Changing the nature of R^1 group by a non-coordinative group to evaluate the impact on antifungal activity.
- Understanding the origin of the antioxidative properties, ligand, or molybdic cluster.

To address these issues, we synthesized 5 new ligands and the corresponding $[Mo^{V}_2O_2S_2]^{2+}$ complexes. To limit the formation of isomers, the substituents R^4 = Me or H, R^3 = H, and R^2 = H were fixed, whereas we varied the nature of aldehyde in R^1. Intuitively, if we want to favour the formation of a single isomer, we can for example introduce steric constraints between ligands. Besides, since R^1 has been shown not to be involved coordinating Mo centres, we don't necessarily need a coordinating group present in R^1. Consequently, we introduced in R^1 position dimethylbenzene group for ligands HL^1 and HL^2, 3- or 5-methoxy-salicyladehyde for H_2L^3 and H_2L^4, and the bulky substituent diphenylamine-benzaldehyde for ligand HL^5 (see Scheme 2). Each of them thus displays bulkier R^1 group than those used in our previous works in the hope of preventing isomers formation upon complexation with $[Mo^{V}_2O_2S_2]^{2+}$. Furthermore, the ligands HL^1 and HL^2 possess a non-coordinative group as R^1, which will permit to complete our previous studies, notably against fungi.

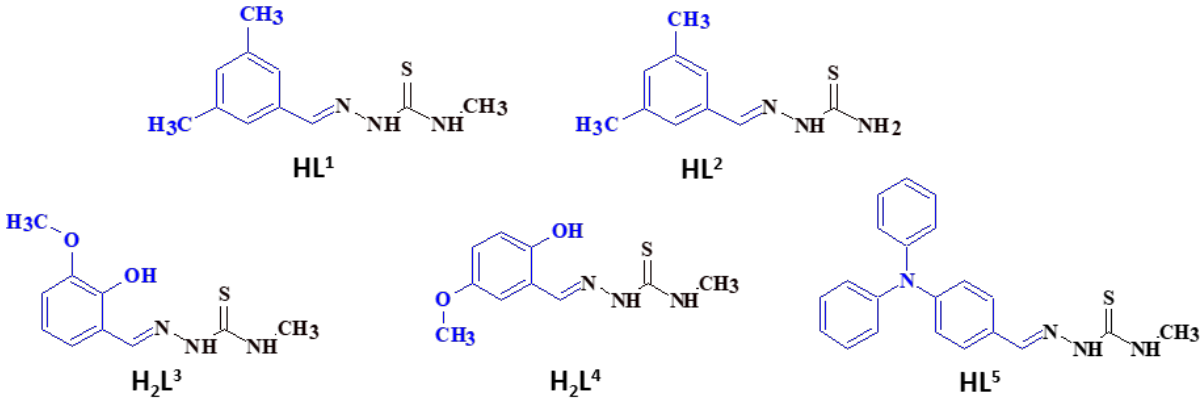

Scheme 2. *Drawing of the ligands used in this study.*

In this paper, a special attention is paid to combining NMR experimental and DFT studies to assess the effect of the variation of R^1 on the number of species formed in solution, so to better understand the preferential formation of *cis* or *trans* isomers. The biological activity as antibacterial, antifungal and antioxidant is evaluated both for ligands and complexes, notably to evidence some selective properties of such class of complexes. DFT calculations were performed on the ligands and *cis* and *trans* isomers of the complexes with the aim to determine the electronic levels and the nature of the frontier orbitals in the ligands and the complexes and to better understand the antioxidant activities of the complexes and to determine the origin of such a behaviour.

1- Experimental section

1.1 Materials and methods

Fourier Transform Infrared (FT-IR) spectra were recorded on a 6700 FT-IR Nicolet spectrophotometer, using diamond ATR technique. The spectra were recorded on solid compounds and ATR correction was applied. **Elemental analyses** were performed by Biocis laboratory, University Paris-Saclay (www.biocis.universite-paris-saclay.fr), Châtenay-Malabry, France. **EDX** measurements were performed on a JEOL JSM 5800LV apparatus.

Electrospray Ionization Mass Spectrometry (ESI-MS) spectra were collected for ligands by using a Q-TOF instrument supplied by WATERS. Samples were solubilized in water at a concentration of 10^{-4} M and were introduced into the spectrometer via an ACQUITY UPLC WATERS system whilst a Leucine Enkephalin solution was co-injected via a micro pump as internal standard.

MALDI-TOF mass Spectrometry. A MALDI-TOF/TOF UltrafleXtreme mass spectrometer (Bruker Daltonics, Bremen) was used for all experiments. Acquisitions were performed in reflector or linear positive ion mode. The laser intensity was set just above the ion generation threshold to obtain peaks with the highest possible signal-to-noise (S/N) ratio without significant peak broadening. The mass spectrometer was externally calibrated using PEG1500 and PEG4500. All data were processed using the program FlexAnalysis (Bruker Daltonics, Bremen). The matrix 1,8,9-anthracenetriol (Dithranol), was purchased from Sigma Aldrich at the highest grade available, and used without further purification. Samples were prepared at a concentration of 60 μM in tetrahydrofuran. The matrix solution was prepared at a concentration of 6 mM in THF with or without addition of a sodium salt. The samples were prepared by mixing the sample solution with matrix solution at a volume ratio of 1:9. After drying, the residues were analyzed by MALDI-TOF technique.

Nuclear magnetic resonance (NMR) ^{1}H and ^{13}C NMR spectra were measured at 298 K on Bruker Avance 300 MHz spectrometer with 5 mm BBI probe head at 9.4 T. All samples were solubilised in DMSO-d_6 deuterated solvent. The ^{1}H spectra were recorded as standard procedure using one pulse sequence at 30° flip angle with 2.8 μs duration pulse time, 2 s recycle delay, 1.6 s for acquisition time, and 8 number of scans. The ^{13}C spectra were obtained with either standard power-gated decoupling or Dept145 pulse sequences, using typically 4.5 s recycle delay, 1.3 s acquisition time, and ca. 8000 number of scans. Chemical shifts are reported

relative to 1% Me_4Si in $CDCl_3$ (^1H and ^{13}C) according to conventional standard. Simulation of NMR spectra were performed by using DMFIT software (free access through the link https ://cemhti.cnrs-orleans.fr/dmfit/).

XRD analysis. Yellow-orange crystals of compound **$[Mo_2O_2S_2(HL^3)_2]$** were obtained by recrystallization from DMSO solutions. The diffraction data were collected on a Bruker Apex Duo diffractometer with MoKα radiation (λ = 0.71073 Å) by doing φ and ω scans of narrow (0.5°) frames at 200 K. Crystals were glued in paratone oil to prevent any loss of crystallization water. An empirical absorption correction was applied using the SADABS program.[35] Structures were solved by direct methods and refined by full-matrix least-squares treatment against $|F|^2$ in anisotropic approximation with SHELX 2014/7 set[36] using ShelXle program.[37] Further details about the crystal structure determinations may be obtained free of charge from the Cambridge Crystallographic Data Centre via www.ccdc.cam.ac.uk/data_request/cif on quoting the depository number CCDC-2191589.

Computational details. The molecular geometry of all the complexes were fully optimized using a Density Functional Theory (DFT) method implemented in the Amsterdam Density Functional package (AMS 2021.101, SCM, Theoretical Chemistry, Vrije Universiteit, Amsterdam, The Netherlands, http://www.scm.com)[38] using the Slater TZP basis set from AMS library. We used the Becke and Perdew exchange-correlation functional (BP86),[39][40] together with the dispersion correction D3 from Grimme.[41] Relativistic corrections are included by the scalar Zero Order Regular Approximation (ZORA).[42] Water solvation effects were considered employing the continuous Conductor like Screening Model (COSMO)[43] using the Klamt atomic radii. Analytical vibrational frequencies were computed for the stationary points to check their nature as minima in the energy surface. NMR chemical shifts were computed, using same functional and basis set as for geometry optimizations, and some values with TZ2P basis set.

A dataset collection of the computational results is available in the ioChem-BD repository and can be accessed via the following link: https://doi.org/10.19061/iochem-bd-1-264.

During the reviewing process this link is not accessible : for reviewers please follow the link https://iochem-bd.iciq.es/browse/review-collection/100/53726/5230d6e20532ea3588a2cc23.

1.2 Protocols of biological tests

1.2.1 Antibacterial and antifungal activity tests

Antibacterial and antifungal activity of the synthesized compounds are assessed using the microdilution broth test, which allows determination of minimum inhibitory concentration (MIC), minimum bactericide concentration (MBC) and the minimum fungicidal concentration (MFC). (Reference Method for Broth Dilution Antifungal Susceptibility Testing of Yeasts; Approved Standard—Third Edition, 2002; Clinical and Laboratory Standards Institute document M27-A3; Methods for Dilution Antimicrobial Susceptibility Tests for Bacteria that Grow Aerobically, Approved Standard, 9th ed, 2012, Clinical and Laboratory Standards Institute). For MIC assays a stock solution (10 mg/mL) of each test compound was prepared in dimethyl sulfoxide (DMSO). This stock solution was then diluted in Muller Hinton Broth (MHB) for bacteria and liquid RPMI (Roswell Park Memorial Institute) 1640 medium with both L-glutamine and 0.165 M MOPS buffer and without sodium bicarbonate was provided (ready for use) for fungi. The next dilutions were made using 2% of peptonate bullion. Plates were covered and incubated on the shaker at 37°C for 24 h (bacteria), 48 h (*Candida* spp.), and 72 h (*Cryptococcus* spp.). MICs were assessed visually after the corresponding incubation period and were taken as the lowest sample concentration at which there was no (or virtually) growth. For the minimum bactericidal concentrations (MBC) determination, 10 µl aliquots from each well that showed no growth of microorganism were plated on Mueller-Hinton Agar or Sabouraud Dextrose Agar and incubated at 37°C for 24 h (bacteria), 48 h (*Candida* spp.), and 72 h (*Cryptococcus* spp.). The lowest concentration that yielded no growth after subculturing

was taken as the MBC or MFC. Furacillinum was used as the standard antibacterial drug and nystatine was used as the standard antifungal drug. All the experiments were carried out in triplicates.

1.2.2 In vitro antioxidant tests

To determine antioxidant capacity, spectrophotometric method was used, where to solutions of specifically coloured free radicals (ABTS radical cation) is added to the experimental substance in different concentrations followed by absorbance measurements.

The chemicals and reagents used were of analytical grade and obtained from Sigma Aldrich: ABTS (2,2'-Azinobis-(3-ethylbenzothiazoline-6-sulfonic acid), *Trolox* (6-hydroxy-2,5,7,8-tetramethychroman-2-carboxylic acid), potassium persulfate ($K_2S_2O_8$). DMSO, methanol, acetate buffered saline solution (pH 6.5) were purchased from local suppliers. Deionized water was obtained by Adrona Crystal E HPLC water treatment system.

The antioxidant activity by the $ABTS^{\bullet+}$ was assessed according to the method described by Re *et al.* with modifications.[44] The $ABTS^{\bullet+}$ radical was formed through the reaction of ABTS solution 7 mM with potassium persulfate solution 140 mM, incubated at 25 °C in the dark for 12–16 h. Once formed, the $ABTS^{\bullet+}$ solution was diluted with acetate buffered saline solution (0,02 M, pH 6.5) to give an absorbance of 0.7 ± 0,01 at 734 nm. Dilutions of *Trolox*, *DOXO* (Doxorubicin) and experimental compounds were prepared in DMSO at concentrations ranging from 0.1 to 100 μM. After that, 20 μL of each experimental compound dilution were transferred in a 96 wells microtiter plate and 180 μL of working solution of $ABTS^{\bullet+}$ were dispensed with dispense module of hybrid reader (BioTek). The mixture was stirred for 15 s. The change in absorbance at 734 nm was measured exactly after 30 min of incubation at 25 °C. Blank samples were run with solvent only, without $ABTS^{\bullet+}$. The decrease in absorbance is expressed as % inhibition, which is calculated from the following formula:

$$((Abs_{control}-Abs_{sample})/Abs_{control})\times 100$$

1.3 Chemicals and syntheses

The sulphurated precursor $K_{1.5}(NMe_4)_{0.5}[I_2Mo_{10}O_{10}S_{10}(OH)_{10}(H_2O)_5].20H_2O$, denoted hereafter Mo_{10}, was prepared as described in the literature[45] and characterized by routine methods (FT-IR and TGA). Starting chemicals were purchased form Aldrich, Alfa Aesar or Acros companies and used without further purification.

1.3.1 Syntheses of ligands

Thiosemicarbazone ligands $HL^{1-2,5}$ and H_2L^{3-4} were prepared according to literature protocols and characterized by FT-IR, ESI-MS, and ^1H and ^{13}C NMR spectroscopy. Ligands are synthesized by condensing aromatic aldehydes with thiosemicarbazides in a molar ratio of 1:1 in methanol or ethanol. The reactant mixture is refluxed for 4 h in the presence of a few drops of acetic acid as a catalyst. The final reaction products are solid. They are isolated by filtration and washed with ethanol or methanol and dried under vacuum.[46] The synthesized ligands were all insoluble in water. However, they have shown higher solubility in polar solvents, such as dimethylformamide (DMF), dimethylsulfoxide (DMSO), and acetonitrile (MeCN).

4-Methyl-3-thiosemicarbazone of 3,5-dimethylbenzaldehyde (HL^1). White powder (yield = 74 %). FT-IR/cm^{-1}, (Diamond ATR)**:** 3294 (m, sh.); 3115 (w); 2980 (w); 1591 (s); 1544 (m, sh.); 1515 (w, sh.); 1424 (s); 1371 (s); 1292 (m); 1242 (w); 1162 (s); 1087 (m); 1036 (m); 957 (m); 941 (vs); 900 (s); 845 (m); 802 (s); 706 (s); 685 (m); 656 (s); 617 (vs); 505 (vs); 448 (s). ^1H NMR: δ ppm (300 MHz/DMSO-d_6): 11.43 (s, 1H); 8.45 (m, 1H); 7.98 (s, 1H); 7.39 (s, 2H); 7.03 (s, 1H); 3.02 (d, 3H); 2.28 (s, 6H). ^{13}C NMR: δ ppm (300 MHz/DMSO-d_6): 177.6; 142.06; 137.72; 134.06; 131.26; 124.90; 30.81; 20.76.

Thiosemicarbazone of 3,5-dimethylbenzaldehyde (HL^2). White powder (yield = 79 %). FT-IR/cm^{-1}, (Diamond ATR)**:** 3392 (w); 3248 (m); 3155 (m); 3025 (s); 2913 (s); 1617 (s);

1599 (w); 1530 (vw); 1458 (s); 1385 (vs); 1364 (s); 1301 (m); 1216 (s, br.); 1175 (s); 1162 (s); 1096 (m); 1059 (s); 996 (vs); 946 (w); 849 (w); 834 (w); 713 (s); 688 (w); 621 (m); 563 (m, br.); 538 (s); 469 (s); 426 (s).^{1}H NMR: δ ppm (300 MHz/DMSO-d_6): 11.30 (s, 1H); 8.20 (s, 1H); 7.96 (s, 2H); 7.39 (s, 2H); 7.00 (s, 1H); 2.26 (s, 6H). ^{13}C RMN: δ ppm (300 MHz/DMSO-d_6): 177.78; 142.50; 137.70; 133.98; 131.32; 125.03; 20.72.

4-Methyl-3-thiosemicarbazone of 2-hydroxy-3-methoxybenzandehyde (H_2L^3). White powder (yield = 96 %). FT-IR/cm^{-1}, (Diamond ATR)**:** 3338 (s); 3305 (w, sh.); 1551 (w, sh.); 1527 (w, sh.); 1479 (w); 1447 (w); 1387 (vs); 1360 (s); 1331 (s); 1268 (w, br.); 1216 (w); 1186 (s); 1166 (s); 1108 (s); 1066 (w); 931 (m); 882 (vs); 831 (vs); 807 (m); 785 (m); 755 (s); 736 (m); 660 (s); 642 (s); 610 (s); 570 (s); 536 (m); 523 (m); 479 (vs); 403 (m). ^{1}H RMN: δ ppm (300 MHz/DMSO-d_6): 11.44 (s, 1H); 9.19 (s, 1H); 8.40 (q, 1H); 8.38 (s, 1H); 7.55 (d, 1H); 6.95 (d, 1H); 6.78 (t, 1H); 3.80 (s, 3H); 3.00 (d, 3H). ^{13}C RMN: δ ppm (300 MHz/DMSO-d_6): 177.49; 147.89; 145.83; 138.76; 120.87; 118.88; 117.99; 112.65; 55.86; 30.80.

4-Methyl-3-thiosemicarbazone of 2-hydroxy-5-methoxybenzandehyde (H_2L^4). White powder (yield = 76 %). FT-IR/cm^{-1}, (Diamond ATR): 3377 (vw, sh.); 3247 (vw, br.); 3012 (m); 2934 (m.); 2832 (s); 1621 (s); 1610 (s); 1578 (s); 1552 (vw, br.); 1518 (w); 1496 (m, br.); 1385 (s); 1369 (s); 1330 (vw, br.); 1262 (vw); 1239 (m); 1189 (m); 1167 (m); 1116 (s); 1089 (m); 1024 (w); 956 (s); 942 (s); 849 (s); 832 (m); 780 (m); 726 (s); 670 (s); 634 (vs); 609 (s); 571 (s); 526 (s); 498 (s); 469 (s). ^{1}H RMN: δ ppm (300 MHz/DMSO-d_6): 11.42 (s, 1H); 9.47 (s, 1H); 8.44 (q, 1H); 8.33 (s, 1H); 7.48 (d, 1H); 6.82 (d, 1H); 6.79 (s, 1H); 3.72 (s, 3H); 3.01 (d, 3H). ^{13}C RMN: δ ppm (300 MHz/DMSO-d_6): 177.27; 152.20; 150.46; 138.51; 120.77; 117.49; 116.72; 109.97; 55.59; 30.75.

4-Methyl-3-thiosemicarbazone of 4-(N,N-diphenylamino)benzaldehyde (HL^5). Yellow powder (yield = 89 %). FT-IR/cm^{-1}, (Diamond ATR)**:** 3370 (s); 3145 (m); 2995 (s); 1586 (vw); 1548 (w); 1505 (m); 1486 (vw); 1448 (vs); 1419 (s); 1382 (s); 1337 (s); 1320 (m);

1292 (m); 1265 (vw); 1165 (m); 1147 (s); 1079 (s); 1036 (s); 995 (vs); 932 (s); 904 (vs); 830 (s); 782 (s); 764 (m); 755 (m); 726 (s); 709 (s); 700 (s); 692 (m); 632 (s); 621 (s); 615 (s); 606 (s); 579 (s, br.); 537 (s); 527 (m); 511 (s); 492 (s); 446 (s); 524 (s); 407 (m). ^{1}H NMR: δ ppm (300 MHz/DMSO-d_6): 11.40 (s, 1H); 9.39 (m, 1H); 7.96 (s, 1H); 7.65 (d, 2H); 7.33 (t, 4H); 7.11 (d, 2H); 7.06 (d, 4H); 6.91 (d, 2H); 2.99 (d, 3H). ^{13}C NMR: δ ppm (300 MHz/DMSO-d_6): 177.36; 148.60; 146.54; 141.38; 129.67; 128.36; 127.65; 124.74; 123.85; 121.49; 30.75.

1.3.2 Syntheses of $[Mo^{V}_2O_2S_2]^{2+}$ complexes

The solid thiosemicarbazone ligand $HL^{1-2,5}$ or H_2L^{3-4} (0.833 mmol) is dissolved in 40 mL of EtOH at 55-60 °C. Freshly prepared 25 mL of aqueous solution of $K_{2-x}(NMe_4)_x[I_2Mo_{10}O_{10}S_{10}(OH)_{10}(H_2O)_5]\cdot 20H_2O$ precursor (250 mg, 0.0833 mmol; 0.417 mmol $[Mo_2O_2S_2(H_2O)_6]^{2+}$ is transferred to the hot thiosemicarbazone solution by dropwise addition. The mixture is stirred continuously and heated to 65 °C for one hour, which leads to the formation of yellow powders. For each synthesis , the yellow product is filtered, washed with water, ethanol, and diethyl ether, and then dried under vacuum.

$[Mo_2O_2S_2(L^1)_2]$. Yellow powder (yield = 90 %). FT-IR/cm^{-1}, (Diamond ATR): 3368 (m); 3336 (m); 2933 (s); 2912 (s); 1579 (vw, sh.); 1447 (s); 1428 (s); 1353 (m); 1296 (vs); 1169 (s); 1072 (m); 1014 (s); 965 (vw, sh.); 951 (m); 901 (vs); 846 (s); 824 (s); 727 (m); 689 (m); 660 (s); 578 (s); 474 (s). ^{1}H RMN: δ ppm (300 MHz/DMSO-d_6): 9.52 (m, 1H); 9.18 (s, 1H); 7.72 (s, 2H); 7.16 (s, 1H); 3.02 (d, 3H); 2.37 (s, 6H). Elemental analysis for $[Mo_2O_2S_2(C_{11}H_{14}N_3S)_2]$ Calc. (found): C 36.26 (36.24); H 3.87 (3.65); N 11.53 (11.46); S 17.60 (17.46). EDX: found (expected): Mo/S = 0.51 (0.50). MALDI-TOF: *m/z* Calc. (found) 729.6 (729.9) for molecular ion $[M+H]^+$ and *m/z* 751.6 (751.9) for $[M+Na]^+$.

$[Mo_2O_2S_2(L^2)_2]$. Yellow powder (yield = 96 %). FT-IR/cm^{-1}, (Diamond ATR): 3499 (m); 3438 (m); 3375 (w); 3325 (m); 1592 (vw, sh.); 1505 (w); 1380 (vs); 1350 (w); 1289 (s); 1163 (s); 1051 (s); 955 (vw, sh.); 848 (s); 813 (vs); 797 (vs); 731 (s); 693 (s); 685 (s); 561 (vs); 550 (vs); 538 (vs); 481 (s); 458 (s). ^{1}H RMN: δ ppm (300 MHz/DMSO-d_6): 9.21 (d, 1H); 9.16 (s, 2H); 7.73 (s, 1H); 7.16 (s, 1H); 2.36 (s, 6H). Elemental analysis for $[Mo_2O_2S_2(C_{10}H_{12}N_3S)_2]$ Calc. (found): C 34.29 (34.12); H 3.45 (3.30); N 12.00 (11.81); S 18.31 (18.37). EDX expected (found): Mo/S = 0.48 (0.50). MALDI-TOF: *m/z* Calc. (found) 701.6 (701.9) for $[M+H]^+$ and *m/z* 723.6 (723.9) for $[M+Na]^+$.

$[Mo_2O_2S_2(HL^3)_2]$. Yellow powder (yield = 63 %). FT-IR/cm^{-1}, (Diamond ATR): 3339 (s); 3306 (w); 1595 (m, br.); 1554 (w, br.); 1527 (w, br.); 1478 (w); 1448 (w); 1387 (vs); 1360 (s); 1331 (s); 1259 (w, br.); 1216 (w); 1186 (s); 1166 (s); 1108 (s); 1067 (w); 957 (m); 931 (m); 882 (vs); 830 (vs); 807 (s); 784 (s); 755 (vs); 736 (m); 642 (s); 610 (s); 571 (m); 537 (s); 523 (s); 479 (s). ^{1}H RMN: δ ppm (300 MHz/DMSO-d_6): 9.62-9.34 (m, 3H); 7.77 (d, 1H); 7.10 (d, 1H); 6.91 (t, 1H); 3.88 (s, 3H); 3.00 (d, 3H). Elemental analysis for $[Mo_2O_2S_2(C_{10}H_{12}N_3SO_2)_2](Mo_{12}O_{12}S_{12}(OH)_{12}(H_2O)_6)_{0.035}(CH_3OH)_{0.5}(H_2O)_{0.5}$ Calc. (found): C 28.60 (28.73); H 3.26 (3.01); N 9.76 (9.96); S 16.46 (16.26). EDX found (expected): Mo/S = 0.53 (0.50). MALDI-TOF: *m/z* Calc. (found) 765.6 (765.8) for $[M+H]^+$ and *m/z* 787.6 (787.8) for $[M+Na]^+$.

$[Mo_2O_2S_2(HL^4)_2]$. Yellow powder (yield = 76 %). FT-IR/cm^{-1}, (Diamond ATR)**:** 3464 (vs); 3247 (vs); 1603 (vw, sh.); 1571 (s); 1493 (w); 1467 (vs); 1451 (vs); 1402 (s); 1333 (m); 1268 (vw); 1220 (vs); 1185 (s); 1164 (s); 1083 (s); 1040 (m); 1021 (s); 963 (m); 950 (m); 865 (vs); 838 (vs); 817 (m); 780 (s); 766 (s); 736 (m); 687 (s); 653 (vs); 596 (vs); 570 (vs); 532 (vs); 477 (s); 394 (s); 342 (s). ^{1}H RMN: δ ppm (300 MHz/DMSO-d_6): 9.81 (s, 1H); 9.56 (q, 1H);

9.49 (s, 1H); 7.71 (d, 1H); 7.00-6.89 (m, 2H); 3.79 (s, 3H); 3.01 (d, 3H). Elemental analysis for $[Mo_2O_2S_2(C_{10}H_{12}N_3SO_2)_2](Mo_{12}O_{12}S_{12}(OH)_{12}(H_2O)_6)_{0.019}(CH_3OH)_{0.8}(H_2O)_{2.5}$ Calc. (found): C 28.30 (28.58); H 3.71 (3.77); N 9.92 (9.62); S 15.22 (12.51). EDX found (expected): Mo/S = 0.52 (0.50). MALDI-TOF: *m/z* Calc. (found) 765.6 (765.8) for $[M+H]^+$ and *m/z* 787.6 (787.8) for $[M+Na]^+$.

$[Mo_2O_2S_2(L^5)_2]$. Yellow powder (yield = 92 %). FT-IR/cm^{-1}, (Diamond ATR): 3296 (s); 3027 (vs); 1589 (vw, sh.); 1508 (s); 1488 (w); 1363 (vs); 1320 (s); 1282 (m); 1269 (m); 1174 (vs); 1079 (s); 1029 (vs); 960 (w); 945 (s); 839 (s); 808 (s); 751 (m); 729 (vs); 714 (vs); 698 (m); 669 (m); 637 (s); 617 (s); 598 (s); 547 (s); 533 (s). ^{1}H RMN: δ ppm (300 MHz/DMSO-d_6): 9.47 (m, 1H); 9.13 (s, 1H); 7.97 (d, 2H); 7.38 (t, 4H); 7.14 (d, 4H); 7.10 (d, 2H); 7.02 (d, 4H); 2.99 (d, 3H). Elemental analysis for $[Mo_2O_2S_2(C_{21}H_{19}N_4S)_2]$ Calc. (found): C 50.10 (49.97); H 3.80 (3.88); N 11.13 (11.07); S 12.74 (12.81). EDX found (expected): Mo/S = 0.46 (0.50). MALDI-TOF: *m/z* Calc. (found) 1007.9 (1007.9) for $[M+H]^+$ and *m/z* 1029.9 (1029.9) for $[M+Na]^+$.

2. Results

2.1. Synthesis

The cyclic compound $K_{2-x}(NMe_4)_x[I_2Mo_{10}O_{10}S_{10}(OH)_{10}(H_2O)_5]$ (denoted Mo_{10}) is used as precursor to obtain the $[Mo^V_2O_2S_2]^{2+}$ cluster. This family of molybdenum cycles are highly labile.[47] Therefore, the Mo_{10} solution must be prepared quickly and immediately mixed with ligands because Mo_{10} precursor can quickly reorganize to give the neutral insoluble compound $[Mo_{12}O_{12}S_{12}(OH)_{12}(H_2O)_6]$.[48] This Mo_{10} cycle possesses 10 hydroxo bridges, which can deprotonate thiosemicarbazone ligands in the water/ethanol reaction medium. Quantitatively, 10 OH^- bridges can react with 10 molecules of thiosemicarbazone ligands. During the

hydrolysis of the cycle, 5 fragments of $[Mo_2O_2S_2]^{2+}$ are obtained which react with the monodeprotonated ligands. As can be seen in Scheme 1, thiosemicarbazone ligands can exist in two forms. It is well known that uncoordinated ligands adopt the thione form (form A in Scheme 1). However, deprotonation generally takes place on the azomethine nitrogen atom, and the coordination of the ligand then takes place in the deprotonated thiolate form B. In this study, we obtained 5 compounds in powder form, which were characterized by FT-IR (see Supporting Information), Elemental Analysis and EDX. These analyses agree with the formation of complexes between the $[Mo_2O_2S_2]^{2+}$ cluster and the monodeprotonated thiosemicarbazone ligands and in particular the formation of neutral complexes of the $[Mo_2O_2S_2(H_nL)_2]$ type (see experimental part). Mass spectrometry by the MALDI-TOF method is thus carried out to confirm the stoichiometry in these complexes.

2.2 MALDI-TOF

MALDI-TOF mass spectrometry has proven to be very effective in characterizing such neutral complexes. Figure 2 shows an example of a spectrum obtained for the compound $[Mo_2O_2S_2(L^5)_2]$, while the other spectra are given in Supporting Information and the data are gathered in Table 1. The complexes obtained are neutral. In all cases, only a few degradation products are observed, and the main peaks correspond to monocationic adducts formed between the expected neutral complexes and an H^+ proton or a Na^+ cation. The simulated isotopic distribution perfectly matches the 1:2 stoichiometry of $[Mo_2O_2S_2(L)_2]$ complexes, in agreement with previous studies by Fuior et al.[33]

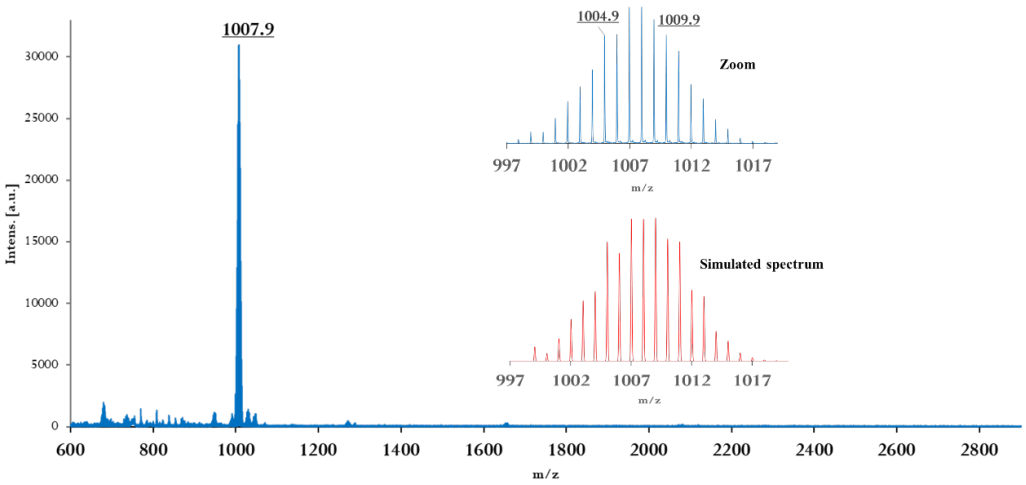

Figure 2. *MALDI-TOF mass spectrum of the compound [$Mo_2O_2S_2(C_{21}H_{19}N_4S)_2$]. The simulated spectrum is obtained with IsoPro3 freeware.*

Table 1. ESI-MS data obtained for the ligands and MALDI-TOF results of the complexes [$Mo_2O_2S_2(H_nL^{1\text{-}5})_2$]

Product	Exp. *m/z*	Assignment	Calc. *m/z*
HL^1	222.1	$[C_{11}H_{15}N_3S]+H^+$	222.3
HL^2	208.0	$[C_{10}H_{13}N_3S]+H^+$	208.3
H_2L^3	240.0	$[C_{10}H_{13}N_3SO_2]+H^+$	240.3
H_2L^4	240.0	$[C_{10}H_{13}N_3SO_2]+H^+$	240.3
HL^5	361.1	$[C_{21}H_{20}N_4S]+H^+$	361.4
$[Mo_2O_2S_2(L^1)_2]$	729.9	$[Mo_2O_2S_2(C_{11}H_{14}N_3S)_2+H]^+$	729.6
	751.9	$[Mo_2O_2S_2(C_{11}H_{14}N_3S)_2+Na]^+$	751.6
$[Mo_2O_2S_2(L^2)_2]$	701.9	$[Mo_2O_2S_2(C_{10}H_{12}N_3S)_2+H]^+$	701.6
	723.9	$[Mo_2O_2S_2(C_{10}H_{12}N_3S)_2+Na]^+$	723.6
$[Mo_2O_2S_2(HL^3)_2]$	765.8	$[Mo_2O_2S_2(C_{10}H_{12}N_3SO_2)_2+H]^+$	765.6
	787.8	$[Mo_2O_2S_2(C_{10}H_{12}N_3SO_2)_2+Na]^+$	787.6
$[Mo_2O_2S_2(HL^4)_2]$	765.8	$[Mo_2O_2S_2(C_{10}H_{12}N_3SO_2)_2+H]^+$	765.6
	787.8	$[Mo_2O_2S_2(C_{10}H_{12}N_3SO_2)_2+Na]^+$	787.6
$[Mo_2O_2S_2(L^5)_2]$	1007.9	$[Mo_2O_2S_2(C_{21}H_{19}N_4S)_2+H]^+$	1007.9
	1029.9	$[Mo_2O_2S_2(C_{21}H_{19}N_4S)_2+Na]^+$	1029.9

2.3 X-Ray Crystal Structure

The **$[Mo_2O_2S_2(HL^3)_2]$** complex solvated with two DMSO molecules crystallizes in a triclinic $P\bar{1}$ space group. The detailed crystallographic data are given in Table 2 and selected distances are listed in Table 3. The molecular structure of the complex is depicted in the Figure 3. The two monodeprotonated bidentate thiosemicarbazone ligands are coordinated in *trans* configuration to $[Mo^V_2O_2S_2]^{2+}$ cluster, through S-thiolate and azomethinic N atoms. This type of coordination leads to a 4-atom ring with Mo(V) metal ions, where the Mo-S and Mo-N distances were found to be 2.441 and 2.136 Å, respectively. The phenolic and imino groups are not involved in coordination conversely to what usually happens in 3d complexes. Both Mo(V) atoms in $[Mo^V_2O_2S_2]^{2+}$ cluster are pentacoordinated with a distorted square pyramidal geometry. The Mo-Mo (2.831 Å), Mo-S (2.302–2.341 Å) and Mo=O (1.675–1.678 Å) bond distances are consistent with the usual ranges observed in the $[Mo^V_2O_2S_2]^{2+}$ cluster.[47][49][50]. The deprotonation of the ligand is confirmed by C-S and C=N bond distances. Thus, the increase in the distance of the C-S bond (1.745 Å) in the complex compared to the C=S in the free ligand (1.695 Å) is accompanied by a shortening of the C-N bond (1.338 Å) between the azomethinic C and the hydrazinic N atoms in the complex compared to C=N double bond in the uncoordinated ligand (1.363 Å)[51]. The crystal packing of the complex is stabilized by intermolecular bonding between DMSO molecules and molecular units (Figure S6, ESI). The oxygen atom of one DMSO molecule is connecting two molecular units by hydrogen bonds with phenol and amino groups: $H12A_{(OH)}\ldots O1D_{(DMSO)}\ldots H1A_{(NHMe)}$ (2.028 and 1.971 Å, respectively). These dimeric assemblies end with hydrogen bonding between oxygen atom of second DMSO molecule and phenol and amino groups of one molecular unit, $H12B_{(OH)}\ldots O1C_{(DMSO)}\ldots H1B_{(NHMe)}$ (2.663 and 1.977 Å respectively).

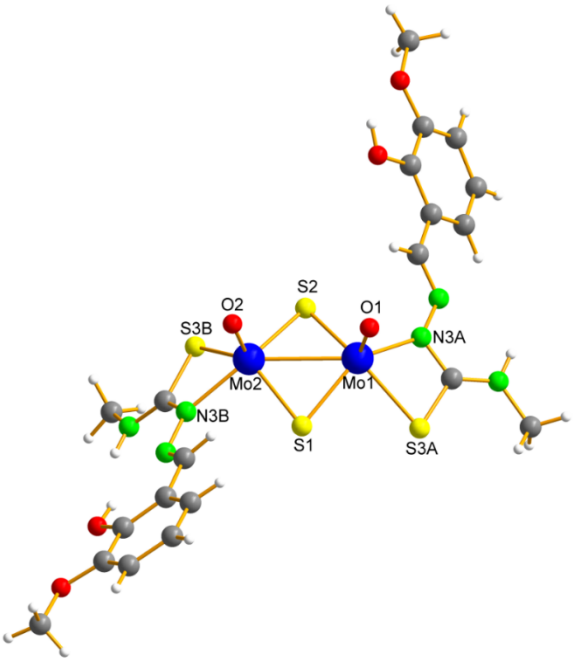

Figure 3. *X-Ray molecular structure of [$Mo_2O_2S_2(HL^3)_2$] complex. Colour code: Mo (blue), C (grey), O (red), N (green), and S (yellow).*

Table 2. Crystallographic data for [$Mo_2O_2S_2(HL^3)_2$]·2DMSO complex

Complex	**[$Mo_2O_2S_2(HL^3)_2$]·2DMSO**
Formula	$C_{24}H_{36}Mo_2N_6O_8S_6$
M (g mol^{-1})	920.83
Crystal system	Triclinic
Space group	$P\bar{1}$
T (K)	220
Crystal	Yellow Parallelepiped
a (Å)	9.8232(3)
b (Å)	12.7500(4)
c (Å)	14.6369(5)
α (°)	93.020(2)
β (°)	101.021(2)
γ (°)	94.990(2)
V ($Å^3$)	1788.07(10)
Z	2
D_{calc} (g cm^{-3})	1.710
Crystal size (mm)	0.28 × 0.18 × 0.10 mm
F(000)	932

μ(Mo-Kα)/Å	0.71073
Reflections collected	70946
Independent reflections (I > 2σ(I))	8345
Parameters	425
Δ(ρ) (e Å^{-3})	1.22 and -0.80
Goodness of fit	1.05
R_1[a]	0.0307 (0.0443)[b]
wR_2[a]	0.0692 (0.0771)[b]

[a] $R = \sum||F_o| - |F_c||/\sum|F_o|$, $wR_2 = [\sum w(F_o^2 - F_c^2)^2/\sum w(F_o^2)^2]^{1/2}$; [$F_o > 4\sigma(F_o)$]. [b] Based on all data.

Table 3. Selected bond lengths around Mo atoms (Å) in $[Mo_2O_2S_2(HL^3)_2]$·2DMSO crystal structure and in molecular structures optimized by DFT calculation

Complexes	Mo-Mo	Mo=O	Mo-N	Mo-S (bridges)	Mo-S (Ligand)	C-S	(N)N=C(S)
Experimental XRD structure							
Trans-$[Mo_2O_2S_2(HL^3)_2]$	2.831	1.678 1.675	2.135 2.137	2.302 2.341 2.303 2.334	2.460 2.441	1.745 1.745	1.330 1.338
Optimized structures by DFT							
cis-$[Mo_2O_2S_2(L^1)_2]$	2.852	1.713 1.714	2.162 2.167	2.351 2.354 2.332 2.344	2.492 2.491	1.752 1.756	1.349 1.345
trans-$[Mo_2O_2S_2(L^1)_2]$	2.852	1.715 1.715	2.150 2.150	2.322 2.365 2.364 2.322	2.486 2.486	1.752 1.752	1.345 1.345
cis-$[Mo_2O_2S_2(L^2)_2]$	2.873	1.713 1.714	2.154 2.159	2.331 2.324 2.343 2.348	2.501 2.503	1.744 1.746	1.343 1.341
trans-$[Mo_2O_2S_2(L^2)_2]$	2.849	1.714 1.714	2.157 2.158	2.364 2.320 2.364 2.321	2.487 2.484	1.751 1.751	1.338 1.338
cis-$[Mo_2O_2S_2(HL^3)_2]$	2.867	1.713 1.714	2.161 2.163	2.353 2.323 2.339 2.345	2.501 2.515	1.749 1.744	1.347 1.351
trans-$[Mo_2O_2S_2(HL^3)_2]$	2.837	1.718 1.720	2.185 2.161	2.369 2.322 2.325 2.358	2.462 2.494	1.752 1.767	1.348 1.339
cis-$[Mo_2O_2S_2(HL^4)_2]$	2.866	1.713 1.714	2.160 2.159	2.335 2.328 2.347 2.351	2.505 2.507	1.748 1.747	1.349 1.349
trans-$[Mo_2O_2S_2(HL^4)_2]$	2.839	1.718 1.719	2.161 2.167	2.357 2.323 2.370	2.494 2.486	1.755 1.752	1.346 1.348

				2.323			
cis-$[Mo_2O_2S_2(L^5)_2]$	2.868	1.714	2.159	2.334	2.501	1.748	1.349
		1.715	2.161	2.342	2.504	1.751	1.345
				2.350			
				2.352			
trans-$[Mo_2O_2S_2(L^5)_2]$	2.852	1.716	2.179	2.324	2.465	1.755	1.345
		1.715	2.161	2.370	2.488	1.767	1.338
				2.322			
				2.372			

2.4. NMR Studies

^{1}H NMR spectra of free ligands and complexes were recorded in DMSO. The example of **$[Mo_2O_2S_2(HL^3)_2]$** complex is given in Figure 4, while the spectra of all other ligands and complexes are given in the Supporting Information (Figure S12-S15). The chemical shifts of the ligands and complexes are reported in Table S1 in the Supporting Information. As a general feature, the ^{1}H NMR spectra of the complexes clearly confirm the deprotonation of the N azomethine NH group of the ligands and the coordination of the ligands to the Mo(V) cluster $[Mo^V_2O_2S_2]^{2+}$. It is worth mentioning that the latter is diamagnetic due to the Mo-Mo bond that realizes the pairing of the two lone electrons in each metal centre. The analysis of the ^{1}H NMR spectra also confirms that the OH functions in the two ligands H_2L^3 and H_2L^4 remain protonated and are not coordinated to Mo, in agreement with Fuior et al.[33] In this previous study, it was shown that depending on the different substituents in position R^3 and R^4, up to 8 isomers can be obtained in solution. We hypothesized that using R^3 = H and R^4 = H or alkyl should limit the number of isomers to at least 2. Moreover, in the present study, the series of 5 ligands aimed to put larger substituents in R^1 or R^2 to promote the formation of a single isomer due to a steric hindrance between the ligands. The analysis of the ^{1}H NMR spectra of the 5 complexes of this study confirms the first hypothesis but it does not allow to form only one species in solution. All spectra can be mainly decomposed into two subspectra displaying the same multiplicities in DMSO. These two sets of NMR signals are assigned to two distinct complexes which are probably the *cis* and *trans* isomers of the complexes.

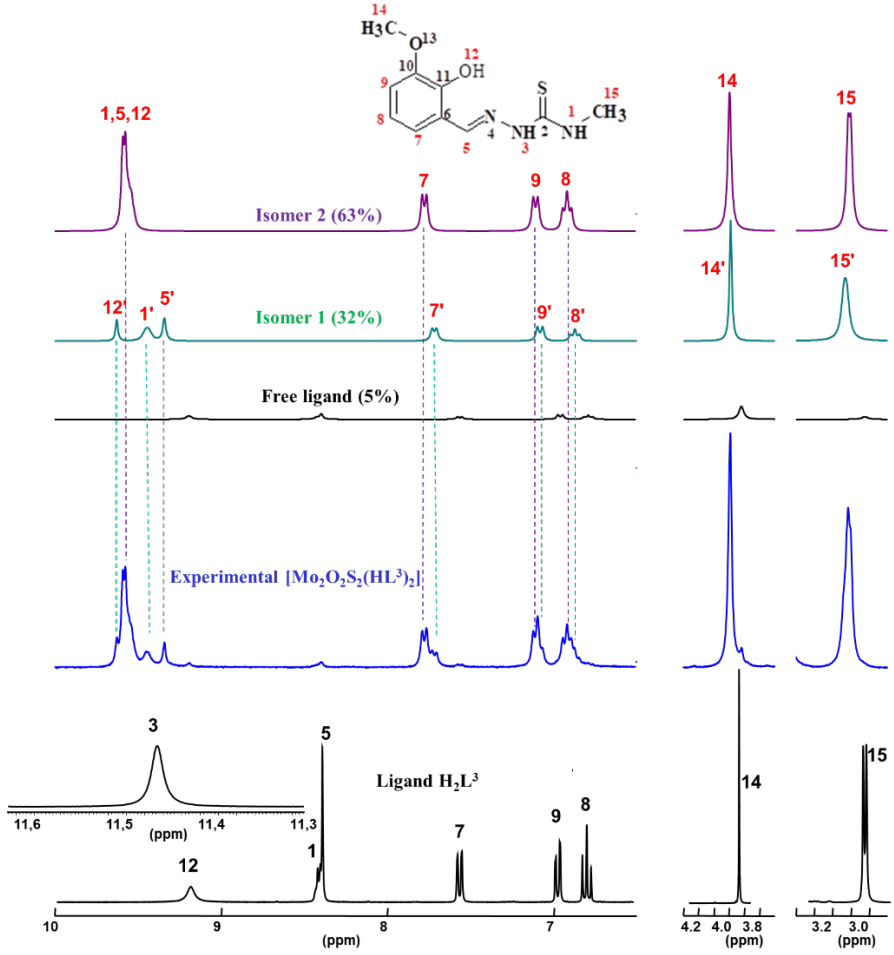

Figure 4. *^{1}H-NMR (DMSO-d_6, 300 MHz) spectra of ligand H_2L^3 (black), complex* ***[Mo$_2$O$_2$S$_2$(HL^3)$_2$]*** *(blue), and the simulated subspectra contained in the experimental spectrum of* ***[Mo$_2$O$_2$S$_2$(HL^3)$_2$]***.

The proportions of the various isomers are indicated on the ^{1}H NMR spectra and at this stage it is difficult to discriminate between the *cis* and *trans* isomers in solution. For example, in the case of the $[Mo_2O_2S_2(HL^3)_2]$ complex, the species distribution for H_2L^3 was 63:32:5 for isomer2:isomer1:free ligand. It was not possible to determine which spectrum corresponds to the *cis* isomer and which spectrum corresponds to the *trans* isomer. These proportions of isomers (and free ligand is so) are found equal to 64:36:0 for $[Mo_2O_2S_2(L^1)_2]$ (Figure S12, ESI), 63:37:0 for $[Mo_2O_2S_2(L^2)_2]$ (Figure S13, ESI), 76:18:6 for $[Mo_2O_2S_2(HL^4)_2]$ (Figure S14, ESI), and 41:59:0 for $[Mo_2O_2S_2(L^5)_2]$ (Figure S15, ESI). DFT calculations were then undertaken on all possible *cis/trans* species, and their conformers aimed at understanding these results.

2.5. DFT Studies

In the absence of additional structural data and aiming to shed light into the preferential formation of *cis* or *trans* isomers, the molecular geometries of all ligands, complexes and a model system were fully optimized by means of a DFT method (see above). We considered a model complex, which consist of the simplest thiosemicarbozane-$Mo_2O_2S_2$ complex, to assess the energy difference between the *cis* and *trans* conformations in the absence of ligands effects (see Figure S16, SI). This preference turned to be quite low (0.65 kcal·mol^{-1}) favouring the *trans* isomer (Table 4).

The series of complexes can be classified in three groups depending on the ligand structure. In the first group we can align ligand HL^1 and HL^2 as well as their respective metal complexes. Both HL^1 and HL^2 have similar structures, differing one of the other on the CH_3 on the N^1 position. None of these structures can form intramolecular hydrogen bonds. Second group is formed by H_2L^3 and H_2L^4 ligands and their metal complexes. Both ligands can form 0, 1 or 2 intramolecular OH-N hydrogen bonds. For this reason, we considered three different conformers for each $[Mo_2O_2S_2(HL^3)_2]$ *cis* and *trans* complexes: conformer 1 (Conf. 1) present zero hydrogen bonds, conformer 2 (Conf. 2) one, and conformer 3 (Conf. 3) two (see Figure S17, SI). The last group includes HL^5 and its metal complexes. In this case, there is no possibility of intramolecular hydrogen bonds, but some π stacking interactions between aromatic rings are possible at the same time.

The *cis* complexes formed with ligands HL^1 and HL^2 are flexible enough to give or not give π-π stacking between aromatic groups in the substituents R^1 (see Figure 5). Consequently, for the $[Mo_2O_2S_2(L^1)_2]$ complex, we also considered two different conformers, one with the rings in parallel position and the other with a CH_3 group pointing towards the centre of the opposite ring. Results of this calculations show no major differences (0.2 kcal·mol-

[1]). The same difference in energy is found in HL^2 *cis* complex. Regarding the *cis* / *trans* preference of $[Mo_2O_2S_2(L^1)_2]$ and $[Mo_2O_2S_2(L^2)_2]$, the data in Table 4 indicates that both species are in equilibrium, with a small preference for the *cis* isomer in both cases.

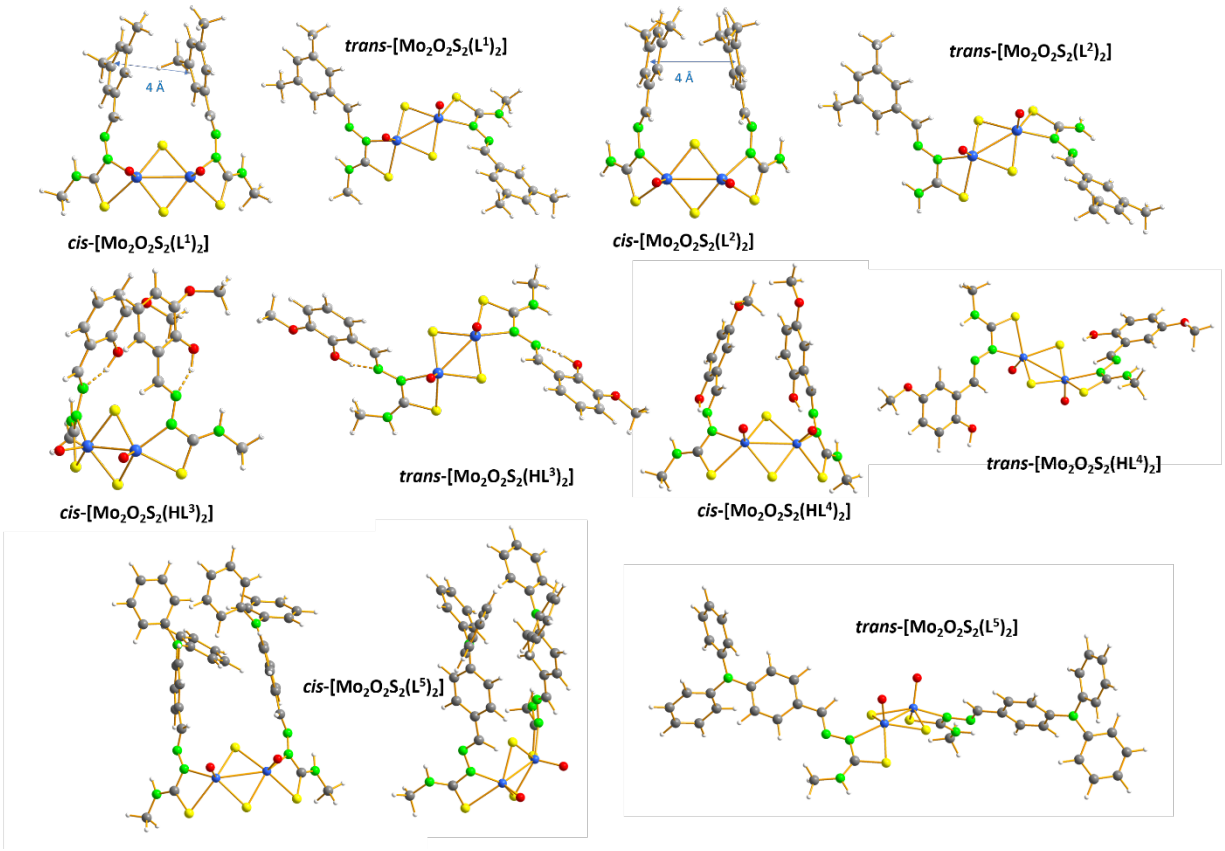

Figure 5. *DFT optimized molecular structures of complexes in cis and trans configurations. Color code: Mo (blue), C (grey), O (red), N (green), and S (yellow).*

The X-Ray characterized complex $[Mo_2O_2S_2(HL^3)_2]$ shows the *trans* disposition, and regarding intramolecular presents conformation Conf.2 as described above, so one OH-N hydrogen bond (see Figure 3 and Figure S17, SI). We considered the three different conformers. The optimized geometries for the complexes in their two most stable isomeric forms are depicted in Figure 5, while selected distances are given in Table 3 in comparison with experimental values. What it can be deduced from Table 3, is that the bond distances obtained by DFT fully agree with the experimental data obtained for compound $[Mo_2O_2S_2(HL^3)_2]$, and also with the previous complexes reported by Fuior et al.[33] In particular, the Mo-Mo distances are fully compatible with a Mo-Mo bond expected for

the $[Mo^{V}O_2S_2]^{2+}$ cluster. This good agreement validates the molecular structures obtained by DFT geometrical optimization. π-π interactions are also found in the *cis*-$[Mo_2O_2S_2(HL^3)_2]$ and *cis*-$[Mo_2O_2S_2(HL^4)_2]$ complexes in addition to the strong intramolecular H-bonds (d_{OH-N}=1.6-1.7 Å) between the non-coordinated phenol groups and iminic N atoms of the ligands. As expected, in all cases the most stable conformers of the *cis* and *trans* complexes are the ones that have two intramolecular hydrogen bonds labelled Conf.3. The preference for the *trans* is small (4 kcal.mol^{-1}) and agreement with the X-Ray structure. The difference between Conf.2 and Conf.3 is also small and could be easily overcome by packing effects. Considering the small energies in play, a solvent like DMSO might interrupt the stabilizing intermolecular interactions and make the *cis* and *trans* complexes equally stable. For $[Mo_2O_2S_2(HL^4)_2]$ we report Conf. 3 for the *cis* and Conf.1 for the *trans*, to show how important are the presence of intermolecular interactions in the stability of those complexes.

For complex *cis*-$[Mo_2O_2S_2(L^5)_2]$, which includes the bulkiest ligand, the three phenyl groups of the one ligand stand parallel to those of the second ligand with C-C distances in the 3.5-3.7 Å range, a distance compatible with π-π stacking interactions between both ligands in this conformation. This stabilizing intramolecular interaction could not exist in the *trans* isomer. Therefore, this would explain why *cis*-$[Mo_2O_2S_2(L^5)_2]$ is thermodynamically more stable than *trans*-$[Mo_2O_2S_2(L^5)_2]$.

For all cases bonding energies show that *cis* / *trans* isomers seem to be in an equilibrium with their corresponding conformers. Intuitively, introducing bulky substituents at the R^1 position in the ligand should increase the steric constraints between the ligands once complexed into the *cis* isomer and thus favour the formation of the *trans* isomer. In fact, as shown in Figure 5, the two ligands are not that close and stabilizing intramolecular

interactions such as π-π stacking interaction between the two ligands are only found in the *cis* isomers, counteracting possible steric repulsions.

Table 4. Total Bonding Energies in kcal·mol^{-1}, HOMO, LUMO and HOMO-LUMO gap energies in eV for ligands (as protonated ligand) and complexes in *cis* and *trans* configurations.

Molecule	Total Bonding Energy (kcal·mol^{-1})	$\Delta E_{cis\text{-}trans} = E_{trans} - E_{cis}$ (kcal·mol^{-1})	HOMO (eV)	LUMO (eV)	HOMO-LUMO gap (eV)
Model *cis*	-4589.87	**-0.65**	-5.703	-3.141	2.562
Model *trans*	-4590.52		-5.773	-3.224	2.549
HL^1	-4159.18	+0.83	-5.40	-2.67	2.73
cis-$[Mo_2O_2S_2(L^1)_2]$	**-9244.78**		-5.47	-3.07	2.40
trans-$[Mo_2O_2S_2(L^1)_2]$	-9243.95		-5.50	-3.15	2.35
HL^2	-3789.30	+0.55	-5.45	-2.71	2.74
cis-$[Mo_2O_2S_2(L^2)_2]$	**-8502.55**		-5.55	-3.11	2.44
trans-$[Mo_2O_2S_2(L^2)_2]$	-8502.00		-5.59	-3.27	2.32
HL^3	-4076.03	-8.02	-5.28	-2.58	2.70
Conf. 1 *cis*-$[Mo_2O_2S_2(L^3)_2]$	-9064.45		-5.47	-3.20	2.27
Conf. 1 *trans*-$[Mo_2O_2S_2(L^3)_2]$	**-9072.47**		-5.35	-3.17	2.16
Conf. 2 *cis*-$[Mo_2O_2S_2(L^3)_2]$	-9071.20	-8.41	-5.53	-3.15	2.38
Conf. 2 *trans*-$[Mo_2O_2S_2(L^3)_2]$	**-9079.61**		-5.32	-3.18	2.14
Conf. 3 *cis*-$[Mo_2O_2S_2(L^3)_2]$	-9079.79	-3.98	-5.52	-3.17	2.35
Conf. 3 *trans*-$[Mo_2O_2S_2(L^3)_2]$	**-9083.77**		-5.29	-3.20	2.09
HL^4	-4075.29	+11.49	-5.11	-2.70	2.41
(Conf.3) *cis*-$[Mo_2O_2S_2(L^4)_2]$	**-9087.44**		-5.12	-3.13	1.99
(Conf.1) *trans*-$[Mo_2O_2S_2(L^4)_2]$	-9075.95		-5.14	-3.17	1.97

HL^5	-6793.26		-4.79	-2.64	2.15
cis-$[Mo_2O_2S_2(L^5)_2]$	**-14519.90**	+11.74	-4.81	-3.05	1.76
trans-$[Mo_2O_2S_2(L^5)_2]$	-14508.16		-4.83	-3.17	1.66
Trolox	-5021.40		-4.86	-1.52	3.33
Rutin	-10494.76		-5.59	-3.07	2.52

DFT calculations of ^{1}H-NMR were carried out for HL^1 and HL^3 ligand and its *cis* and *trans* isomers. Chemical shifts for the different hydrogen's signals are collected in Table 5 in comparison with isomers 1 and 2 experimentally observed (see Figure 4, Figure S12 and Table S2, SI). Unfortunately, no major differences between the *cis* and *trans* isomers could be observed and DFT calculation cannot help to assign isomers on the NMR spectra. On the other hand, important differences were found between the signals of different conformers. The existence of OH-N hydrogen bonds implies a huge displacement of the OH H(12) signal, from 6-7 ppm for the cases without, to 12-14 ppm for hydrogen bonded protons. Therefore, in addition to the *cis/trans* isomerism the computed NMR data suggest that several conformers could be present in solution. The presence or absence of hydrogen bonds in positions N^1 and N^3 largely affects the N-H signals. This could explain why there is a 2ppm mismatch between DFT results and experimental chemical shifts for those exchangeable protons. DMSO solvent molecules interact both with the ligands and the metal complexes, as it is depicted in the crystal structure of trans-$[Mo_2O_2S_2(L^3)_2]$ complex indeed (see Figure S6). The solvent may form different hydrogen bonds with the N^3 proton of the free ligands, and also with N^1 proton in both the ligand and the complexes. Overall, for the C-H protons, the computed chemical shifts reproduce rather well the experimental values.

Table 5. Experimental and calculated chemicals shifts (in ppm) for HL^1 and H_2L^3 ligands and their metal complexes. Note that for some complexes both ligands are not identical. In this case, two/three sets of chemical shifts are obtained.

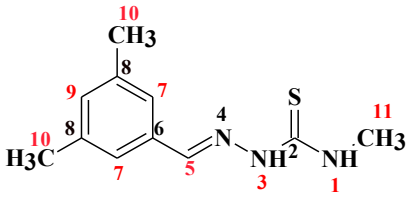

			H(1)	H(3)	H(5)	H(7)	H(8)	H(9)	H(10)	H(11)	H(12)	H(14)	H(15)
	DFT	HL^1	8.6	9.5	8.2	7.7/8.4	-	7.8	2.7/2.8	3.7	-	-	-
		Cis-$[Mo_2O_2S_2(L^1)_2]$	8.5/8.7	-	9.6/9.8	7.8/8.2/8.4	-	7.7/8.0	2.7/3.0	3.5	-	-	-
		trans-$[Mo_2O_2S_2(L^1)_2]$	8.8/8.9		9.4/9.5	8.1/8.7	-	8.0	2.9	3.5	-	-	-
	NMR	HL^1	8.45	11.43	7.98	7.39	-	7.03	2.28	3.02	-	-	-
		Isomer 1	9.41	9.35	7.73	-	-	7.12	2.34	3.04	-	-	-
		Isomer 2	9.52	9.19	7.71	-	-	7.17	2.38	3.02	-	-	-

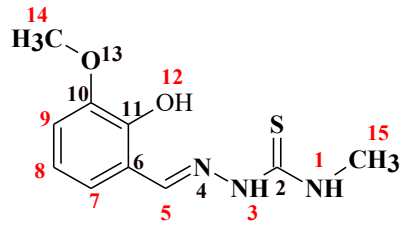

	DFT	HL^3	6.5	9.3	8.5	7.4	7.4	7.4	-	-	14.1	4.2	3.2
		Conf 1 cis-$[Mo_2O_2S_2(L^3)_2]$	8.2	-	9.8	8.3	7.4	7.6	-	-	6.6	4.4	3.3
		Conf 1 trans-$[Mo_2O_2S_2(L^3)_2]$	7.3	-	9.8	8.0	7.5	7.5	-	-	6.9	4.2	3.5
		Conf 2 cis-$[Mo_2O_2S_2(L^3)_2]$	7.6	-	9.6	7.5	7.2	7.7	-	-	13.0/6.3	4.3	3.1
		Conf 2 trans-$[Mo_2O_2S_2(L^3)_2]$	6.8	-	9.5	7.8	7.5	7.5	-	-	13.3/7.0	4.2	3.6
		Conf 3 cis-$[Mo_2O_2S_2(L^3)_2]$	7.6	-	9.4	7.6	7.2	7.6	-	-	12.8	4.2	3.2
		Conf 3 trans-$[Mo_2O_2S_2(L^3)_2]$	6.8	-	9.3	7.6	7.5	7.5	-	-	13.4	4.2	3.5
	NMR	HL^3	8.40	11.44	8.38	7.55	6.78	6.95	-	-	9.19	3.80	3.00
		Isomer 1	9.44	-	9.33	7.71	6.88	7.07	-	-	9.62	3.89	3.01
		Isomer 2	9.58	-	9.58	7.77	6.91	7.11	-	-	9.58	3.89	3.01

The HOMO and LUMO orbitals of ligands and complexes are depicted in Figure 6 and Table S3 (Supporting Information). For complexes formed with ligands HL^1 and HL^2, the HOMO and LUMO orbitals are delocalized on the entire molecules, but the contribution of the ligands appears stronger for HOMO, while it is the reverse for the LUMO, which shows a stronger contribution on the cluster $[Mo_2^{V}O_2S_2]^{2+}$. In the case of the ligands H_2L^3, H_2L^4 and HL^5, the difference between the ligand and the cluster is emphasized since the contribution of the cluster to the HOMO orbital becomes negligible while its contribution to the LUMO orbital becomes major. It means that the reduction of such complexes and thus the addition of electrons within the LUMO will mainly occur on the cluster while the oxidation, a loss of electron from HOMO, will mainly takes place on the ligands. Furthermore, values of Table 4 also evidence that the levels of HOMO and LUMO of the ligands can be tuned trough the nature of substituents and that the coordination to the cluster $[Mo_2^{V}O_2S_2]^{2+}$ induces a stabilization of the HOMO in comparison with the uncoordinated ligands.

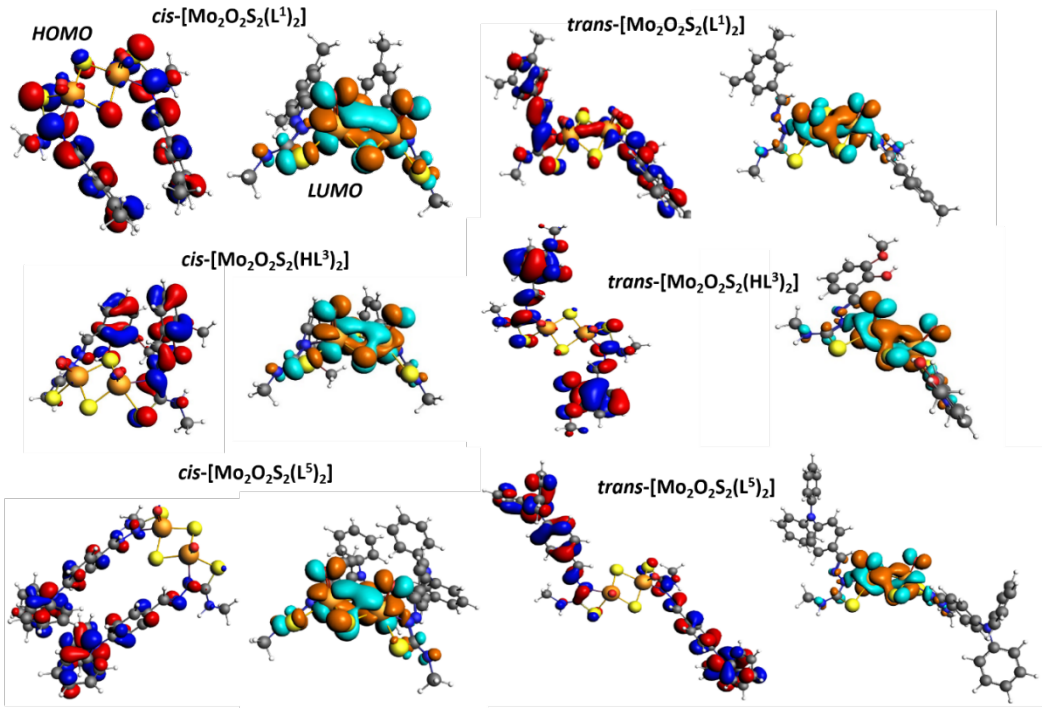

Figure 6. *Representation of the HOMO (left) and LUMO (right) frontiers orbitals for cis and trans isomers of complexes $[Mo_2O_2S_2(L^1)_2]$, $[Mo_2O_2S_2(HL^3)_2]$ and $[Mo_2O_2S_2(L^5)_2]$.*

2.6. Biological activity

2.6.1 Antibacterial activity

The antimicrobial activity of the 5 synthesized complexes and the ligands was tested against representative gram-positive (G+) microorganisms (*Staphylococcus aureus* ATCC 25923 and *Bacillus cereus* ATCC 11778) and gram-negative (G-) microorganisms (*Acinetobacter baumannii* BAA-747 and *Escherichia coli* ATCC 259). The results of the research demonstrated that they have no activity against the studied microorganisms.

2.6.2 Antifungal activity

The antifungal activity of $[Mo_2^{V}O_2S_2]^{2+}$ complexes with thiosemicarbazone ligands and with "classical" ligands L-histidine, L-cysteine, nitrilotriacetate, and EDTA against *Cryptococcus neoformans* and *Candida albicans* was recently reported by Fuior et al.[11][34] With classical ligands, no activity was measured against *Candida albicans*.[11] On the contrary, when thiosemicarbazone complexes are tested, the activity of complexes against *Candida albicans* with ligands possessing a pyridine ring as R^1 group show interesting values of MIC in the range 3.9-7.8 µg/mL, while the ligand bearing quinoline, phenol, thiophen and furan derivatives are not or poorly active[34]. The complexes with classical ligands remain not or poorly active against *Cryptococcus neoformans,* while the thiosemicarbazone complexes tested by Fuior et al. appear highly efficient on *Cryptococcus neoformans* (MIC in the range 0.49-31.25 µg/mL), whatever the nature of the thiosemicarbazone ligand[34]. These results suggest that the ligand should play a crucial role for the antifungal activity of the $Mo_2O_2S_2$-based complexes.

To bring more element for understanding this behaviour, we investigated the 5 ligands alone and the corresponding complexes formed with $[Mo_2^{V}O_2S_2]^{2+}$. The results are gathered in Table

6 in comparison with some selected previous results of Fuior et al.[11][34] (for clarity, ligands from previous study are drawn in Scheme 3).

Table 6. Results of antifungal activity against *Cryptococcus neoformans*. NA: No Activity; MIC: minimum inhibitory concentration; MFC: minimum fungicidal concentration; MFC/MIC: < 2 is fungicidal, >2 is fungistatic and ≥32 is resistant; FA: fungicidal activity.

Product	***Cryptococcus neoformans* CECT 1043**			
	MIC, mg/mL	MFC, mg/mL	MFC/MIC	FA
HL^1	NA	NA	-	-
$[Mo_2O_2S_2(L^1)_2]$	0.008	0.008	1	fungicidal
HL^2	NA	NA	-	-
$[Mo_2O_2S_2(L^2)_2]$	0.004	0.004	1	fungicidal
H_2L^3	NA	NA	-	-
$[Mo_2O_2S_2(HL^3)_2]$	0.016	0.016	1	Fungicidal
H_2L^4	NA	NA	-	-
$[Mo_2O_2S_2(HL^4)_2]$	0.016	0.016	1	fungicidal
HL^5	NA	NA	-	-
$[Mo_2O_2S_2(L^5)_2]$	NA	NA	-	-
$[Mo_2O_2S_2(LHis)_2]$[11]	0.500	0.500	1	fungicidal
$K_2[Mo_2O_2S_2(LCys)_2]$[11]	NA	NA	-	-
$K_2[Mo_2O_2S_2(HNTA)_2]$[11]	0.250	0.250	1	fungicidal
$K_2[Mo_2O_2S_2(EDTA)]$[11]	0.016	0.016	1	fungicidal
$[Mo_2O_2S_2(L^a)_2]$[34]	0.002	-	-	-
$[Mo_2O_2S_2(L^b)_2]$[34]	0.002	-	-	-
$[Mo_2O_2S_2(HL^i)_2]$[34]	0.004	-	-	-
$[Mo_2O_2S_2(H_2L^j)_2]$[34]	0.0005	-	-	-
$[Mo_2O_2S_2(H_2L^k)_2]$[34]	0.004	-	-	-
$[Mo_2O_2S_2(L^m)_2]$[34]	0.002	-	-	-
$[Mo_2O_2S_2(L^n)_2]$[34]	0.031	-	-	-
Nystatin	0.032	0.032	1	fungicidal

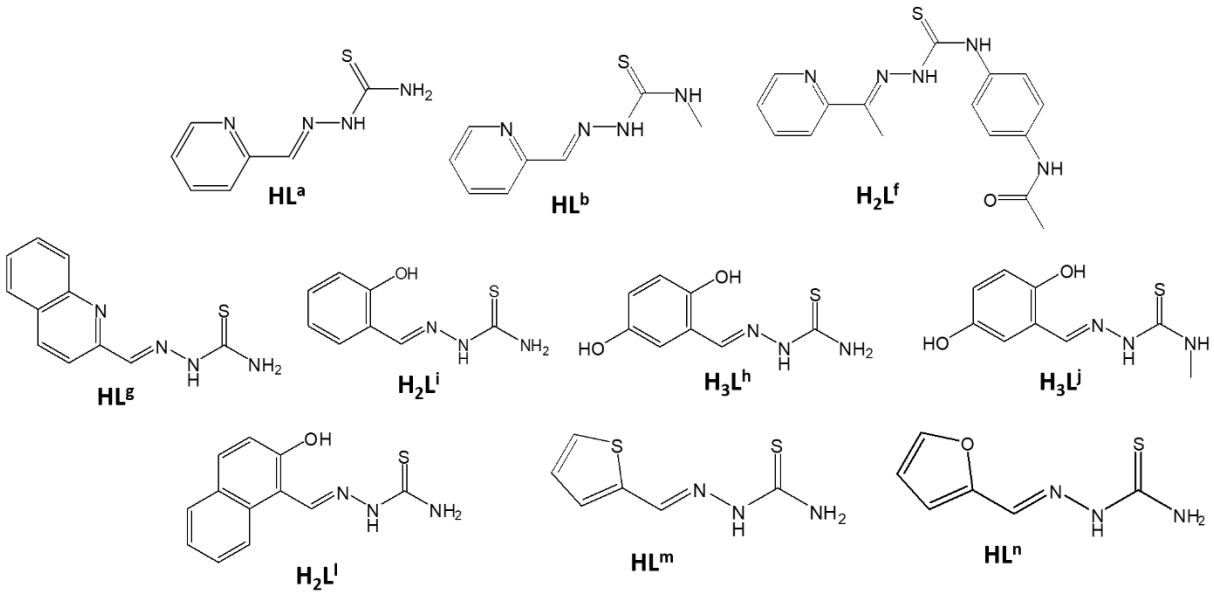

Scheme 3. *Structures of the ligands used in a previous study*[34].

Interestingly, the non-coordinated thiosemicarbazone ligands HL^1-HL^5 are all inactive against both *Cryptococcus neoformans* and *Candida albicans.* Similarly, the complexes $[Mo_2O_2S_2(L^1)_2]$, $[Mo_2O_2S_2(L^2)_2]$, $[Mo_2O_2S_2(HL^3)_2]$, $[Mo_2O_2S_2(HL^4)_2]$ and $[Mo_2O_2S_2(L^5)_2]$ are also inactive on *Candida albicans.*

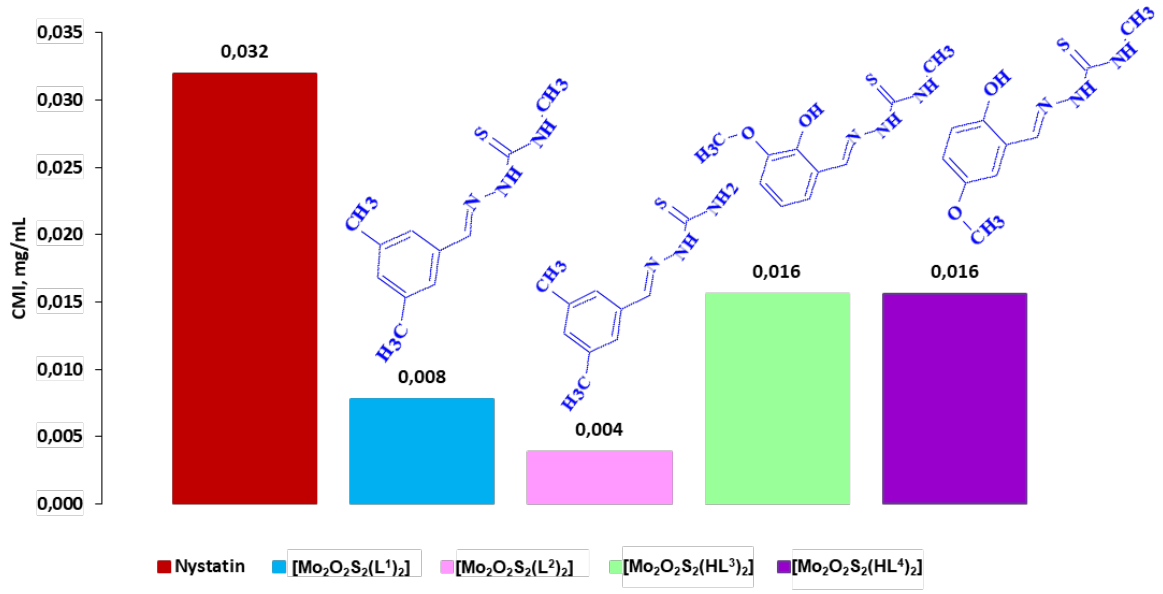

Figure 7. *Antifungal activity of complexes $[Mo_2O_2S_2(H_nL^{1-4})_2]$, n = 0 – 1 against Cryptococcus neoformans.*

Conversely, the activity of complexes $[Mo_2O_2S_2(L^1)_2]$, $[Mo_2O_2S_2(L^2)_2]$, $[Mo_2O_2S_2(HL^3)_2]$, and $[Mo_2O_2S_2(HL^4)_2]$ on *Cryptococcus neoformans* is higher than the reference compound Nystatin (see Figure 7 and Table 5) and of the same order than the $Mo_2O_2S_2$-based thiosemicarbazone complexes previously reported[34]. However, the last complex $[Mo_2O_2S_2(L^5)_2]$ appears inactive. These results demonstrate i) that the activity of the $Mo_2O_2S_2$-based thiosemicarbazone complexes are probably due to the coordinated ligands, ii) that the association of certain thiosemicarbazone ligands with the $[Mo_2O_2S_2]^{2+}$ cluster leads to synergistic systems that are highly active against *Cryptococcus neoformans* and iii) that the activity of the complexes can be partially tuned through the choice of the group R^1 on the ligand but the activity is not lost when R^1 is a non-coordinative group. Moreover, when comparing the complexes $[Mo_2O_2S_2(L^1)_2]$ and $[Mo_2O_2S_2(L^2)_2]$, it is found that the complex with $-NH_2$ is more active than its counterpart with $NH-CH_3$. In the case of complexes $[Mo_2O_2S_2(HL^3)_2]$ and $[Mo_2O_2S_2(HL^4)_2]$, it was found that the position of the $-OCH_3$ group does not influence the antifungal activity.

Finally, these studies performed against *Candida albicans* and *Cryptococcus neoformans* evidence a selective fungicidal activity of the $Mo_2O_2S_2$-based thiosemicarbazone complexes of this study against fungi of the species *Cryptococcus neoformans*.

2.6.3 Antioxidative properties

Free radicals are involved in many major physiological processes in living organisms, causing aging of living beings and development of various diseases. Therefore, antioxidants have the potential to protect cells, tissues and prevent aging of the body. According to previous studies, the molybdenum fragment $[Mo_2O_2S_2]^{2+}$ is known as an active redox centre, and Mo(V) atoms can be oxidized to Mo(VI).[5][52][53] Besides, previous studied by Fuior et al. reported interesting antioxidative properties of $[Mo^V_2O_2S_2]^{2+}$-based complexes, especially L-histidine and L-cysteine ligands, while complexes with ligands such as EDTA or HNTA and $[Mo^V_2O_4]^{2+}$-based

complexes were inactive,[11] thus suggesting that this process could be localized on the $[Mo^{V}_2O_2S_2]^{2+}$ cluster. To our knowledge there is no data reported so far in the literature about other Mo(V) complexes. However, Eglence-Bakir et al. reported some series of complexes of general formula $[Mo^{VI}O_2(L)(solvent)]$ where L is a tridentate thiosemicarbazone (ONN or ONS) ligand.[26][54]–[56] They evidenced not only antioxidative properties of ligands alone but also antioxidative capacities for the corresponding complexes with $[Mo^{VI}O_2]^{2+}$ moiety. For these complexes, the activity is necessarily localized on the ligand and the antioxidative capacity of ligands and complexes are usually comparable to the reference compound TROLOX. But the activity clearly depends on the method used (ABTS or DPPH), the nature of the ligands and substituents in the ligands, the coordination mode of the ligands, the solvent, and the presence or not of protons in the ligands and/or complexes. In some series, the complexes have a lower IC_{50} than ligands,[55][56] while the opposite is true in other series.[26][54]

In this study, we measured the antioxidant activity by the ABTS method for ligands and complexes in comparison with the reference compounds TROLOX and RUTIN. The results are gathered in Figure 8 and in Table 7.

The five thiosemicarbazone ligands in this study show comparable or superior antioxidant capacity to TROLOX. In particular, the two ligands H_2L^3 and H_2L^4 bearing phenolic groups were found to be the best candidates among the five ligands. Comparison between HL^1 and HL^2, which differ only by one methyl group on the terminal amine function, shows slightly higher activity for HL^2 with the terminal $-NH_2$ group compared to HL^1 with the terminal -NHMe group. This may suggest that protons have a beneficial effect, as observed in the tests with DPPH radicals, but not with ABTS to our knowledge.[56]

Interestingly, the complexes formed with the $[Mo^{V}_2O_2S_2]^{2+}$ cluster appear to be much more active against ABTS with an IC_{50} in the range 2.05-3.48 µM, which translates to a TEAC (Trolox Equivalent Antioxidant Capacity, TEAC > 1 means “more active than Trolox”) in the

range 7.56-12.83. These results are similar to the data obtained with L-cysteine ligand, i.e., IC_{50} = 28.9 μM, and its corresponding complex $[Mo^{V}_2O_2S_2(LCys)_2]^{2-}$ with IC_{50} = 1.9 μM (TEAC = 13.84)[11] and are also in agreement with previous study of Fuior et al. in which the activity of ligand was only partially reported[34].

In contrast to the studies of Eglence-Bakir et al. on Mo(+VI)-thiosemicarbazone complexes, both the ligands and the $[Mo^{V}_2O_2S_2]^{2+}$ cluster can be active in our complexes due to the lower oxidation state of the metal centre. Nevertheless, DFT calculation evidences that i) the HOMO orbitals are mainly centred on the ligands in the complexes, and ii) the HOMO-LUMO gap systematically decreases from ligands to the complexes (see Table 4). Therefore, the redox process is most likely centred on the thiosemicarbazone ligands and coordination with $[Mo^{V}_2O_2S_2]^{2+}$ results in a perturbation of the energy levels that exalt the activity of the ligands. It must be also the case of the previously reported complex $[Mo^{V}_2O_2S_2(LCys)_2]^{2-}$ in which the L-cysteine ligand is also probably the centre of the antioxidative activity of the complex.[11]

Table 7. *Antioxidant activities for ligands and $Mo_2O_2S_2$ complexes against ABTS*

Compounds	IC_{50} (μM)	TEAC[a]
HL^1	27.88±0.35	0.94
HL^2	21.62±0.39	1.22
H_2L^3	7.74±0.05	3.40
H_2L^4	9.81±0.03	2.68
HL^5	21.17±0.42	1.24
L-histidine[11]	>100	-
L-cysteine[11]	28.9±1.0	0.91
$[Mo_2O_2S_2(L^1)_2]$	2.74±0.04	9.60
$[Mo_2O_2S_2(L^2)_2]$	2.05±0.36	12.83

$[Mo_2O_2S_2(L^3)_2]$	2.14±0.05	12.29
$[Mo_2O_2S_2(L^4)_2]$	3.00±0.89	8.77
$[Mo_2O_2S_2(L^5)_2]$	3.48±0.66	7.56
$[Mo_2O_2S_2(Lhis)_2]$[11]	7.00±0.40	3.76
$K_2Mo_2O_2S_2(Lcys)_2]$[11]	1.9±0.2	13.84
Trolox	26.30±0.70	1
Rutin	20.70±0.12	1.27

a. TEAC = ratio of the activity Trolox on the activity of a compound X; TEAC = 1 means similar activity; TEAC > 1 means "more active than Trolox"; TEAC < 1 means "less active than Trolox".

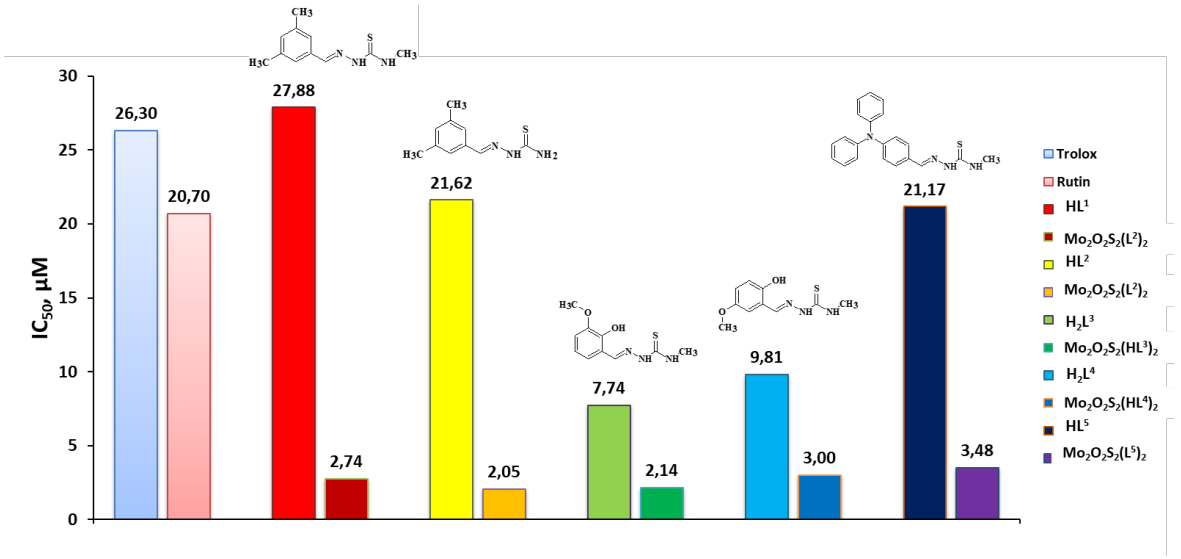

Figure 8. *Antioxidant activities (ABTS) for complexes $[Mo_2O_2S_2(H_nL^{1-5})_2]$, n = 0–1 and ligands in comparison with TROLOX and RUTIN references.*

3. Conclusions

In this study, we synthesized five new complexes associating novel thiosemicarbazone ligands to the cluster $[Mo_2O_2S_2]^{2+}$. The complexes were characterized in the solid state and in solution by various analytical techniques including X-ray diffraction, MALDI-TOF mass spectrometry, and NMR spectroscopy. The results showed the formation of mixture of isomers in solution, consisting mainly of *trans* and *cis* configurations in complexes of 1:2 (metal cluster:ligand)

stoichiometry. DFT calculations revealed that, in most of the cases, the *cis* configuration is favoured due to the stabilizing effect of π-π stacking of the aromatic moieties present in the ligands. Therefore, to address the issue of mixture of isomers, other synthetic strategies must be developed, such as the use of bis-thiosemicarbazone ligands. This work is currently in progress.

The antibacterial, the antifungal and the antioxidative activities of ligands and complexes were studied. We did not evidence any activity against bacteria. In contrast, selective fungicidal activity against fungus *Cryptococcus neoformans* CECT 1043 was observed for all complexes, while the ligands alone were inactive. Finally, the antioxidative capacity of ligands and complexes was evaluated on ABTS radicals. High activity was measured for the ligands alone and this activity was even stronger when these ligands are complexed with the cluster $[Mo_2O_2S_2]^{2+}$. DFT calculations confirmed that the redox process is most likely takes place on the ligands, and that complex formation significantly reduces the HOMO-LUMO gap, further facilitating electron transfer.

Acknowledgements

University of Versailles, the "Institut Universitaire de France, IUF" and the CNRS are gratefully acknowledged for financial support. DC gratefully acknowledge Campus France for Excellence Eiffel grants as well as State University of Moldova for funding her PhD thesis. This work is supported by the "ADI 2019" project funded by the IDEX Paris-Saclay, ANR-11-IDEX-0003-02, "Joint research projects AUF-MECR 2020-2021" funding program, and National Agency for Research and Development (ANCD) of the Republic of Moldova (Project No **20.80009.5007.10** and Project No **20.80009.7007.12**), which are gratefully acknowledged. This study results from an International collaboration supported by IRN-CNRS 2019-2023

Supporting Information

The Supporting Information contains, FT-IR spectra (Figure S1); experimental and simulated MALDI-TOF spectra of complexes not shown in the main text (Figures S2-S5); a view of interaction between complex and DMSO within the structure of complex $[Mo_2O_2S_2(HL^3)_2]$ (Figure S6); a summary of NMR data for ligands and complexes (Tables S1-S2); ^{13}C NMR spectra of ligands (Figures S7-S11); deconvoluted ^{1}H NMR spectra of complexes not shown in the main text (Figures S12-S15); pictures of structures optimized by DFT and HOMO and LUMO orbitals for ligands and complexes (Figures S16-S17, Table S2).

References

[1] R. Hille, *Trends Biochem. Sci.* **2002**, *27*, 360.
[2] R. Hille, T. Nishino, F. Bittner, *Coord. Chem. Rev.* **2011**, *255*, 1179.
[3] R. Hille, R. Mendel, *Coord. Chem. Rev.* **2011**, *255*, 991.
[4] B. Spivack, Z. Dori, *J. Chem. Soc. Chem. Commun.* **1970**, 1716.
[5] V.R. Ott, D.S. Swieter, F.A. Schultz, *Inorg. Chem.* **1977**, *16*, 2538.
[6] B. Spivack, Z. Dori, *Coord. Chem. Rev.* **1975**, *17*, 99.
[7] J. Gretarsdottir, I. Lambert, S. Sturup, S. Suman, *ACS Pharmacol. Transl. Sci.* **2022**, *5*, 907.
[8] S.G. Suman, J.M. Gretarsdottir, P.E. Penwell, J.P. Gunnarsson, S. Frostason, S. Jonsdottir, K.K. Damodaran, A. Hirschon, *Inorg. Chem.* **2020**, *59*, 7644.
[9] S.G. Suman, J.M. Gretarsdottir, T. Snaebjornsson, G.R. Runarsdottir, P.E. Penwell, S. Brill, C. Green, *J. Biol. Inorg. Chem.* **2014**, *19*, S760.
[10] J.M. Gretarsdottir, S. Jonsdottir, W. Lewis, T.W. Hambley, S.G. Suman, *Inorg. Chem.* **2020**, *59*, 18190.
[11] A. Fuior, A. Hijazi, O. Garbuz, V. Bulimaga, L. Zosim, D. Cebotari, M. Haouas, I. Toderas, A. Gulea, S. Floquet, *J. Inorg. Biochem.* **2022**, *226*.
[12] J.S. Casas, M.S. Garcia-Tasende, J. Sordo, *Coord. Chem. Rev.* **2000**, *209*, 197.
[13] T.S. Lobana, R. Sharma, G. Bawa, S. Khanna, *Coord. Chem. Rev.* **2009**, *253*, 977.
[14] E. Pahontu, I. Usataia, V. Graur, Y. Chumakov, P. Petrenko, V. Gudumac, A. Gulea, *Appl. Organomet. Chem.* **2018**, *32*, e4544.
[15] R.B. Singh, H. Ishii, *Crit. Rev. Anal. Chem.* **1991**, *22*, 381.
[16] L.N. Suvarapu, A.R. Somala, J.R. Koduru, S.O. Baek, V.R. Ammireddy, *Asian J. Chem.* **2012**, *24*, 1889.
[17] K.L. Summers, *Mini-Rev. Med. Chem.* **2019**, *19*, 569.
[18] Z.-G. Jiang, M.S. Lebowitz, H.A. Ghanbari, *Cns Drug Rev.* **2006**, *12*, 77.
[19] H. Beraldo, D. Gambino, *Mini-Rev. Med. Chem.* **2004**, *4*, 31.
[20] B. Shakya, P.N. Yadav, *Mini-Rev. Med. Chem.* **2020**, *20*, 638.

[21] E. Pahontu, M. Proks, S. Shova, G. Lupascu, D.-C. Ilies, S.-F. Barbuceanu, L.-I. Socea, M. Badea, V. Paunescu, D. Istrati, A. Gulea, D. Draganescu, C.E.D. Pirvu, *Appl. Organomet. Chem.* **2019**, *33*, e5185.
[22] E. Pahontu, D.-C. Ilies, S. Shova, C. Oprean, V. Paunescu, O.T. Olaru, F.S. Radulescu, A. Gulea, T. Rosu, D. Draganescu, *Molecules* **2017**, *22*, 650.
[23] T. Rosu, E. Pahontu, S. Pasculescu, R. Georgescu, N. Stanica, A. Curaj, A. Popescu, M. Leabu, *Eur. J. Med. Chem.* **2010**, *45*, 1627.
[24] G. Balan, O. Burduniuc, I. Usataia, V. Graur, Y. Chumakov, P. Petrenko, V. Gudumac, A. Gulea, E. Pahontu, *Appl. Organomet. Chem.* **2020**, *34*, e5423.
[25] H.A. El-Ghamry, M. Gaber, T.A. Farghaly, *Mini-Rev. Med. Chem.* **2019**, *19*, 1068.
[26] S. Eglence-Baker, O. Sacan, M. Sahin, R. Yanardag, B. Ulkuseven, *J. Mol. Struct.* **2019**, *1194*, 35.
[27] V. Vrdoljak, I. Đilović, M. Rubčić, S. Kraljević Pavelić, M. Kralj, D. Matković–Čalogović, I. Piantanida, P. Novak, A. Rožman, M. Cindrić, *Eur. J. Med. Chem.* **2010**, *45*, 38.
[28] S. Celen, S. Eglence-Bakir, M. Sahin, I. Deniz, H. Celik, I. Kizilcikli, *J. Coord. Chem.* **2019**, *72*, 1747.
[29] J. Pisk, B. Prugovecki, D. Matkovic-Calogovic, R. Poli, D. Agustin, V. Vrdoljak, *Polyhedron* **2012**, *33*, 441.
[30] V. Vrdoljak, D. Milic, M. Cindric, D. Matkovic-Calogovic, J. Pisk, M. Markovic, P. Novak, *Z. Anorg. Allg. Chem.* **2009**, *635*, 1242.
[31] V. Vrdoljak, J. Pisk, B. Prugovecki, D. Matkovic-Calogovic, *Inorganica Chim. Acta* **2009**, *362*, 4059.
[32] V. Vrdoljak, D. Milic, M. Cindric, D. Matkovic-Calogovic, D. Cincic, *Polyhedron* **2007**, *26*, 3363.
[33] A. Fuior, D. Cebotari, M. Haouas, J. Marrot, G. Espallargas, V. Guerineau, D. Touboul, R. Rusnac, A. Gulea, S. Floquet, *ACS Omega* **2022**, *7*, 16547.
[34] A. Fuior, D. Cebotari, O. Garbuz, S. Calancea, A. Gulea, S. Floquet, *Inorganica Chim. Acta* **2023**, *548*, 121372.
[35] G. M. Sheldrick, **1997**.
[36] G.M. Sheldrick, *Acta Crystallogr. Sect. C Struct. Chem.* **2015**, *71*, 3.
[37] C.B. Hübschle, G.M. Sheldrick, B. Dittrich, *J. Appl. Crystallogr.* **2011**, *44*, 1281.
[38] G. te Velde, F. Bickelhaupt, E. Baerends, C. Guerra, S. Van Gisbergen, J. Snijders, T. Ziegler, *J. Comput. Chem.* **2001**, *22*, 931.
[39] A. Becke, *Phys. Rev. A* **1988**, *38*, 3098.
[40] J. Perdew, *Phys. Rev. B* **1986**, *33*, 8822.
[41] S. Grimme, J. Antony, S. Ehrlich, H. Krieg, *J. Chem. Phys.* **2010**, *132*.
[42] E. Vanlenthe, E. Baerends, J. Snijders, *J. Chem. Phys.* **1993**, *99*, 4597.
[43] A. Klamt, *J. Phys. Chem.* **1995**, *99*, 2224.
[44] R. Re, N. Pellegrini, A. Proteggente, A. Pannala, M. Yang, C. Rice-Evans, *Free Radic. Biol. Med.* **1999**, *26*, 1231.
[45] E. Cadot, B. Salignac, J. Marrot, A. Dolbecq, F. Secheresse, *Chem. Commun.* **2000**, 261.
[46] E. Pahontu, V. Fala, A. Gulea, D. Poirier, V. Tapcov, T. Rosu, *Molecules* **2013**, *18*, 8812.

[47] J.-F. Lemonnier, S. Duval, S. Floquet, E. Cadot, *Isr. J. Chem.* **2011**, *51*, 290.
[48] E. Cadot, B. Salignac, S. Halut, F. Secheresse, *Angew. Chem.-Int. Ed.* **1998**, *37*, 611.
[49] A. Hijazi, J.C. Kemmegne-Mbouguen, S. Floquet, J. Marrot, J. Fize, V. Artero, O. David, E. Magnier, B. Pegot, E. Cadot, *Dalton Trans.* **2013**, *42*, 4848.
[50] A. Hijazi, J.C. Kemmegne-Mbouguen, S. Floquet, J. Marrot, C.R. Mayer, V. Artero, E. Cadot, *Inorg. Chem.* **2011**, *50*, 9031.
[51] V. Vrdojak, M. Cindric, D. Milic, D. Matkovic-Calogovic, P. Novak, B. Kamenar, *Polyhedron* **2005**, *24*, 1717.
[52] J.C. Kemmegne-Mbouguen, S. Floquet, D. Zang, A. Bonnefont, L. Ruhlmann, C. Simonnet-Jegat, X. Lopez, M. Haouas, E. Cadot, *New J. Chem.* **2019**, *43*, 1146.
[53] J.C. Kemmegne-Mbouguen, S. Floquet, E. Cadot, *Comptes Rendus Chim.* **2021**, *24*, 91.
[54] S. Eglence, M. Sahin, M. Ozyurek, R. Apak, B. Ulkuseven, *Inorganica Chim. Acta* **2018**, *469*, 495.
[55] S. Eglence-Bakir, M. Sahin, M. Zahoor, E. Dilmen-Portakal, B. Ulkuseven, *Polyhedron* **2020**, *190*, 114754.
[56] S. Eglence-Bakir, M. Sahin, M. Ozyurek, B. Ulkuseven, *Polyhedron* **2021**, *209*.